Cell. Mol. Biol. (ISSN: 1165-158X)

Journal Homepage: www.cellmolbiol.org

Cellular and Molecular Biology

Original Article

# Computational insights into inhibiting EphA2: Integrating structure-based virtual screening, docking, and molecular dynamics simulations for small molecule discovery

**Mohd Nehal[1], Jahanarah Khatoon[1], Salman Akhtar[2], Mohammad Kalim Ahmad Khan[2*]**

[1] *Department of Biosciences, Integral University, Lucknow, 226026, Uttar Pradesh, India*
[2] *Department of Bioengineering, Integral University, Lucknow, 226026, Uttar Pradesh, India*

**Article Info**

**Article history:**

**Received:** August 24, 2023
**Accepted:** April 08, 2024
**Published:** August 31, 2024

Use your device to scan and read the article online

**Abstract**

Elevated expression and dysfunction of ephrin type A receptor-2 (EphA2) have been implicated in the initiation and progression of cancer, metastasis, and unfavorable clinical outcomes. A promising strategy to counteract this dysregulation involves the development of small-molecule inhibitors that target EphA2. Our study focuses on this objective. To initiate Structure-Based Virtual Screening (SBVS), we leveraged an advanced online platform, the Mcule database, which houses an extensive collection of millions of chemical compounds. Using drug similarity filters, we efficiently identified ten thousand potential hits. By further refining the selection through toxicity profiling, we prudently narrowed down the candidates to a more manageable set of 100 molecules. Using the Mcule Single Click, DockThor, and SwissDock tools, we conducted multi-scoring docking assessments of thirty-seven compounds that satisfied the ADME standards. A comprehensive evaluation of Gibbs binding free energy terms, as derived from these docking tools, facilitated the identification of top-ranking docking hits. Remarkably, among the known inhibitors, dasatinib displayed the most robust binding to EphA2 with an average ΔG of -9.0 kcal/mol. Intriguingly, alternatives have emerged in recent years. Notably, small molecules such as Mcule-1579910267 (ΔG: -9.3 kcal/mol), Mcule-1893218381 (ΔG: -9.2 kcal/mol), Mcule-3981378344 (ΔG: -9.3 kcal/mol), and Mcule-8617639093 (ΔG: -9.1 kcal/mol) exhibited a notably strong binding affinity to EphA2, rivaling dasatinib. Subsequently, the four leading ligands along with dasatinib were selected for the MD simulations. Our rigorous analyses during the MD simulation phase encompassing RMSD, RMSF, SASA, ΔGsolv, and Rg underscored the favorable stability of Mcule-8617639093. This compelling evidence ultimately signifies the potential for selective EphA2 inhibition.

**Keywords:** EphA2, MD simulation, Small molecule inhibitor, Cancer, RTKs

## 1. Introduction

Receptor Tyrosine Kinases (RTKs), which are cell surface receptors, play crucial roles in regulating fundamental cellular processes, embryonic development, and progression of several types of cancer [1]. Upon binding of signaling molecules, RTKs initiate the formation of cross-linked dimers by associating with neighboring RTKs. The Ephrin Receptor (Eph) is one of the most important classes of RTKs and is characterized by its transmembrane structure, which includes an extracellular domain for ligand binding and an intracellular domain. When an Eph receptor binds to a ligand, it activates kinase activity, leading to autophosphorylation and activation of cellular reactions, such as differentiation, migration, and proliferation. Eph signaling affects various biological processes, including cell proliferation, migration, invasion, cell-cell adhesion, and cell repulsion [2-9].

The Eph receptor family is divided into two subfamilies, EphA and EphB. In humans, nine EphAs (EphA1-8 and EphA10) and five EphBs (EphB1-4 and EphB6) interact with the ligands Ephrin-A and Ephrin-B, respectively. Because the ligands are membrane-bound, the Eph receptor can initiate both forward and reverse signaling. In several types of cancer, including liver, melanoma, lung, colon, prostate, gastric, and breast cancers, both EphA and EphB classes are overexpressed [10].

EphA2, which is mapped to chromosome 1p36 in humans, is predominant in proliferating epithelial cells in adults. Although EphA2 and most Eph kinases have been primarily investigated in developing embryos, EphA2 remains prevalent in adult epithelial tissues. Its exact role is still being elucidated, but it is believed to regulate processes, such as proliferation, differentiation, and invasion. Recent studies indicate EphA2's presence in multiple cancers, including lung, colorectal, cervical, ovarian, and breast cancer. When interacting with its preferred ligand

* Corresponding author.
E-mail address: mkakhan@iul.ac.in (M. K. A. Khan).
**Doi:** http://dx.doi.org/10.14715/cmb/2024.70.8.3

Ephrin-A1, EphA2 appears to inhibit tumor growth; however, its overexpression has been implicated in the progression of malignancy [11].

EphA2's binding to its ligand inhibits pathways like JAK/STAT3, integrin signaling, ERK, and PI3K [12-15] (Figure 1). Notably, the overexpression of EphA2 predicts poor prognosis and reduced survival rates in patients with cancer. Moreover, EphA2 targets the p53 protein family, prompting apoptosis when overexpressed [13,14]. Driven by an improved understanding of cancer biology and significant research breakthroughs, efforts are underway to identify precisely designed target-focused anticancer therapeutics. This pursuit involves identifying small molecules that can curb the oncogenic properties of EphA2, including reducing its expression, promoting degradation, and obstructing endogenous activation. This study highlights EphA2 as a therapeutic target specific to cancer cells, with implications for various cancer types. During cancer progression, EphA2 overexpression can trigger ligand-independent pro-oncogenic activation; however, ligand stimulation can counteract these effects [16].

The pursuit of stabilizing novel biomarkers with specific functionality holds great promise for precise interventions in the treatment and prevention of breast cancer. From this perspective, the identification of novel targets that govern cell proliferation and apoptosis in cancerous cells has emerged as a potent strategy for addressing breast cancer. By establishing novel biomarkers and discerning therapeutic compounds against these targets, the impact of such research could be made global in scale.

This study highlights EphA2's increasing potential as a favorable regulator of cell cycle components and a prospective focal point for the selective elimination of malignant cells. However, a comprehensive understanding of EphA2's underlying mechanism is crucial. Towards this direction, the study focused on the identification of investigational EphA2 inhibitors employing a synergistic approach that integrates ADME target-driven screening, multifaceted scoring docking, molecular interactions, dynamics simulations, and principal component analysis.

## 2. Materials and methods

### 2.1. Retrieval and optimization of protein 3D structure

The three-dimensional crystal structure (2.85 Å) of human EphA2 was acquired from the RCSB Protein Data Bank (PDB) [17]. To prepare the structure for docking simulations, heteroatoms, ions, and water molecules were removed, leaving only the apoprotein component. This refined three-dimensional dataset was utilized for molecular interaction studies with ligand molecules. Optimization and energy minimization of the EphA2 three-dimensional structure were accomplished using the CHARMm force field, facilitated by appropriate algorithms [18–20].

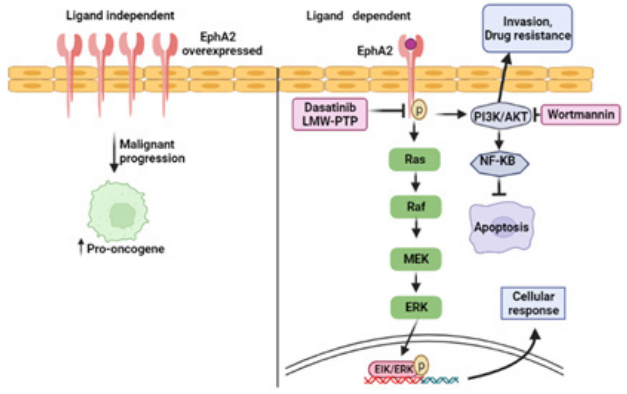


**Fig. 1.** Dynamic interplay of EphA2 overexpression and ligand stimulation in cancer cells.

### 2.2. Structure-Based Virtual Screening

The high-throughput structure-based virtual screening of small molecules was carried out using the MCULE online platform. The SBVS workflow incorporated the RO5 criteria, with parameters such as sample size, diversity selection, and similarity threshold carefully defined. The execution of SBVS was facilitated by employing the Open Babel linear fingerprint search algorithm.

### 2.3. Retrieval and optimization of EphA2 inhibitors

The SDF (Standard Data Format) structures of ligands, including Doxazosin (CID-3157), Dasatinib (CID-3062316), Wortmannin (CID-312145), Sorafenib (CID-216239), and Vemurafenib (CID-42611257), were downloaded from the PubChem database [21–23]. The BIOVIA Discovery Studio Visualizer was used to convert the SDF structures into PDB-3D formats. Optimization and minimization of the energy of each ligand followed a process similar to that applied to the EphA2 protein.

### 2.4. Toxicity Filtration

To expedite the ligand selection process, the MCULE platform's "toxicity checker" feature of the MCULE platform was employed to conduct toxicity filtration. This step was aimed at reducing the number of ligands in the roster. It is worth mentioning that the specific structural characteristics of molecules can contribute to their toxicity. Therefore, the elimination of intricate compounds was performed to minimize potential issues related to toxicity, selectivity, and pharmacokinetics. This selection process was based on the principles of SMILES Arbitrary Target Specification (SMARTS), which utilizes a framework based on a Simplified Molecular Input Line Entry System (SMILES). SMILES expresses the computer-compatible chemical configurations of molecules and is an extension of the SMARTS concept [24–26].

### 2.5. ADME Prediction

The Absorption, Distribution, Metabolism, and Excretion (ADME) process is essential for reducing attrition in the drug discovery process by refining potential chemical candidates. Therefore, it is critical to conduct ADME filtration before initiating clinical studies. During this process, ligand hits that meet the toxicity criteria are carefully examined across a range of ADME attributes, including physicochemical characteristics, lipophilicity, pharmacokinetic traits, drug-likeness, and medicinal chemistry descriptors. The SwissADME tool was used to evaluate attributes [27].

### 2.6. Computational Docking

The integration of AutoDock Vina into the MCULE drug discovery platform (https://mcule.com/), utilization of the DockThor tool from the DockThor-virtual screening web server (https://dockthor.lncc.br/v2/), and engagement of SwissDock, a resource provided by the Swiss Institute of Bioinformatics (SIB) (http://www.swissdock.ch/), col-

lectively facilitated molecular interaction investigations between EphA2 and hits from structure-based virtual screening (SBVS). The goal was to obtain comprehensive insights into binding interactions. By employing these tools, the average Gibbs free energy (ΔG) terms yielded by the selected docking methodologies were harnessed to identify consensus docking hits. This approach aimed to consolidate the findings from the multiple docking tools, thereby enhancing the reliability of the obtained results.

#### *2.6.1. AutoDock Vina*

The AutoDock Vina (ADV) interface was used to import the dock-prepared PDB structure of EphA2. To ensure comprehensive coverage of the protein's binding site region, an AutoGrid setup was configured with a grid size of 40 Å along each of the x-, y-, and z-axes. A specific grid box was defined to encompass the protein's binding center, with variable grid points set for the x-(-78.001 Å), y-(-8.336 Å), and z-axes (88.329 Å). Default parameters were applied for ADV, including a maximum of two binding modes per ligand and exhaustiveness setting of 1. To identify the optimal binding affinities and positions for each ligand docked within EphA2's active site, the minimum free energy of binding (ΔG) was selected as the discriminating parameter. This approach aims to identify the most favorable binding interactions [28-32].

#### *2.6.2. DockThor*

DockThor is a non-covalent molecular docking tool developed by the Molecular Modeling of Biological Systems Group (Brazil). It operates using a ligand topology file and specific input data for the protein, including the atom types and partial charges from the MMFF94S49 force field. The ligand input was generated using the MMFFLigand tool, which incorporates partial charges and atom types using the MMFF94S force field, identifies rotatable bonds and terminal hydroxyl groups, and calculates the necessary properties to assess intramolecular interactions. The grid box's central point and size along the x-, y-, and z-axes were maintained similar to those in ADV, with default settings applied for the spacing between consecutive grids and attributes of the genetic algorithm, including the number of evaluations, population size, number of runs, and run seed. Similar to ΔG, the DockThor scoring mechanism represents the binding affinity and ranking of various ligand molecules, allowing for the comparison and assessment of ligand-binding interactions [33-38].

#### *2.6.3. SwissDock*

SwissDock is a web-based docking service and user interface developed by the Swiss Institute of Bioinformatics (SIB) to showcase the molecular interactions between ligands and target proteins of biological relevance. It utilizes a hybrid evolutionary EADock dihedral space sampling (DSS) algorithm that is seamlessly integrated with the CHARMm force field to calculate the energy and supervision coordinates. SwissDock conducts both local docking, where binding poses are confined within a designated area, and blind docking, which narrows down binding modes around neighboring regions of the target-binding pockets. The calculations were further facilitated by SwissDock's employment of a fast analytical continuum treatment of solvation (FACTS) model for precise binding pose calculations and subsequent clustering. The most energetically favorable binding modes obtained from the docking process, where ligand molecules are placed within the binding pocket of the target protein, were selected for a more in-depth investigation of the molecular interactions. This approach aims to identify the most promising binding configurations for further studies [39, 40].

### 2.7. Molecular Dynamics simulation

A 50-nanosecond molecular dynamics (MD) simulation was performed to evaluate the structural stability of the docked complexes. The GROMACS 5.1.2 software was utilized for the simulation, focusing on EphA2 complexes docked with Dasatinib, Mcule-3981378344, Mcule-1579910267, Mcule-1893218381, and Mcule-8617639093. The simulation was conducted at 300 Kelvin using the molecular mechanics (MM) method. Ligand extraction from the docked complexes was performed using the gmx grep module, and the topology and force field parameters for the ligands were obtained using the CGENFF server. The pdb2gmx modules in GROMACS were employed to create EphA2 topologies, incorporating ligands with data from the CGenFF server [42–44]. Subsequently, the protein-ligand systems were subjected to a 50 ns MD simulation, maintaining uniform conditions at 1 bar and 300 K. To analyze the simulation results, various parameters such as Root Mean Square Deviation (RMSD), Root Mean Square Fluctuation (RMSF), Solvent Accessible Surface Area (SASA), Free energy, Radius of Gyration, and Hydrogen bonds of the docked molecules were calculated using the respective GROMACS modules: gmx rmsd, gmx rmsf, gmx sasa, gmx energy, gmx gyrate, and gmx hydrogen bond [41, 45-46].

## 3. Results

The primary objective of this study was to identify novel inhibitors of EphA2 using the SBVS process, drawing from the extensive MCULE database library of over 5 million ligand molecules. Of these, 1,023,219 were selected for their promising features in relation to EphA2. Following the initial SBVS, the top-ranked hits were subjected to a series of rigorous analyses, including toxicity screening using the toxicity checker, Swiss-ADME filtration, and a multi-scoring docking approach employing AutoDock Vina, DockThor, and Swiss ADME. ΔG values were assessed to ensure comparability with known target protein inhibition. Additionally, a 50 ns molecular dynamics simulation was performed to evaluate the stability of the chosen compounds. The comprehensive workflow encompassing these steps, as shown in Figure 2, aimed to identify potent EphA2 inhibitors with potential for further exploration and development.

### 3.1. Toxicity Risk Evaluation

The issues of molecular toxicity and poor pharmacokinetics in clinical drug candidates pose a significant challenge, resulting in significant attrition during the later stages of the drug development process, which can be costly. In the early stages of small-molecule drug discovery, it is essential to effectively filter out compounds that contain carcinogenic, mutagenic, and toxic moieties as well as detrimental scaffolds and toxicophores.

In light of Mcule's toxicity risk assessment, only 37 compounds were found to be suitable as potential drug candidates, while the remaining ligands were deemed un-

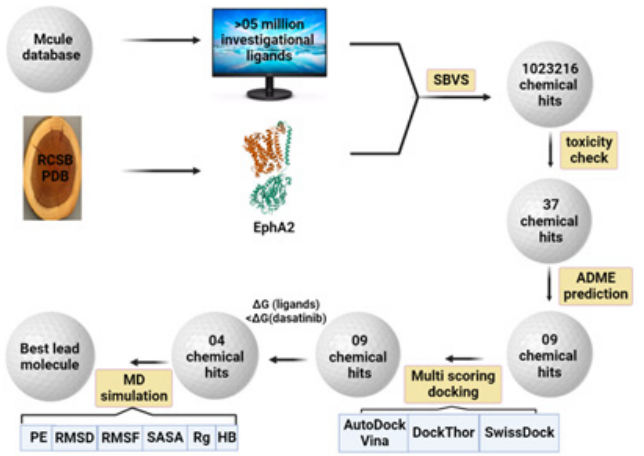


**Fig. 2.** An overview of the structure-based virtual screening approach to identify potential inhibitor molecules targeting EphA2.

suitable and eliminated. Mcule's toxicity checker uses a robust SMARTS algorithm to examine specific chemical patterns within a virtual library of small molecules. This strategic approach prevents potentially toxic compounds from being included in the hit identification list, thereby conserving resources, minimizing costs, and saving valuable time that might otherwise be spent on unsuitable chemical entities [47].

## 3.2. ADME prediction

### *3.2.1. Brain Or IntestinaL EstimateD (BOILED)-Egg model*

The efficacy of the Brain Or Intestinal Estimated Permeation technique (BOILED-egg) in translating molecular designs for drug discovery has been established [31]. BOILED-egg, originally used in CADD to predict Human Gastrointestinal Absorption (HIA) and blood-brain barrier (BBB) permeability, offers a comprehensible graphical approach. The BBB serves as a robust defence mechanism in the brain. The model consists of two components: the yellow yolk represents the physicochemical space for probable BBB permeability, and the white yolk represents the most likely absorption site in the gastrointestinal tract. Successful nontoxic chemical hits were exclusively located within these physicochemical regions for BBB permeability and HIA absorption. These hits outperformed those of the selected inhibitors.

Molecules within the yellow yolk demonstrated a pronounced inclination for BBB penetration, whereas those in the white region displayed a heightened propensity for HIA. Figure 3 illustrates the P-gp-positive and P-gp-negative molecules as blue and red dots, respectively. In contrast, the gray area indicates limited absorption and restricted brain access. The BOILED-egg model employs WLOGP and TPSA parameters to define lipophilicity and apparent polarity [48-50].

For instance, the inhibitor dasatinib, positioned outside the egg, indicated modest absorption yet managed BBB penetration, although it was effluxed by P-gp. Analysis of BOILED-Egg plots revealed 14 compounds as P-gp-positive, while the remaining 37 compounds adhered to the ADME filtration criteria

of BOILED-Egg. Notably, ligand hits originating from the brain (depicted as blue dots) were excluded from the molecular interaction investigation.

### *3.2.2. Physiochemical Properties*

Pharmacokinetics and toxicity of a drug are significantly influenced by its physicochemical attributes. Key molecular and physicochemical descriptors, such as molecular weight (MW), rotatable bonds (RB), hydrogen bond acceptors (HBA), hydrogen bond donors (HBD), molar refractivity (MR), and polar surface area (PSA), play crucial roles in predicting the ADME characteristics of potential ligand molecules. SwissADME employs OpenBabel v2.3.0 to calculate these ADME properties. All 37 ligand hits that successfully passed the BOILED-Egg model exhibited physicochemical properties within the acceptable ranges. The molecular weights of these compounds, listed in the table, vary from 280.32 g/mol to 526.51 g/mol. These selected compounds conform to distinct criteria for oral bioavailability; for instance, dasatinib, a reference compound, possesses more than five rotatable bonds, whereas the evaluated compounds possess fewer than 5.

Among the 37 compounds, the range of TPSA values spans from 34.62 to 148.24Å², with Mcule-7595714167 demonstrating the lowest value of 34.62Å² TPSA. The prediction of TPSA parameters aids in understanding the passive molecular transport of lead compounds. The molar refractivity (MR) was calculated using the Lorenz-Lorentz formula, which represents a constitutive-additive feature influencing both drug-receptor interactions and molecular volume [51-55]. As outlined in Table 1, MR values vary from 144.83 to 70.70, with Mcule-1991062471 displaying the highest MR (144.83) and Mcule-2449737562 having the lowest MR (70.70). The specific physicochemical characteristics of the small molecules and inhibitors that passed the BOILED-Egg criteria are summarized in Table 1.

### *3.2.3. Lipophilicity*

The most critical molecular property in pharmacology is lipophilicity, which significantly influences several key aspects such as solubility, absorption, plasma protein binding, metabolic clearance, distribution volume, interactions with enzymes and receptors, clearance through bilia-

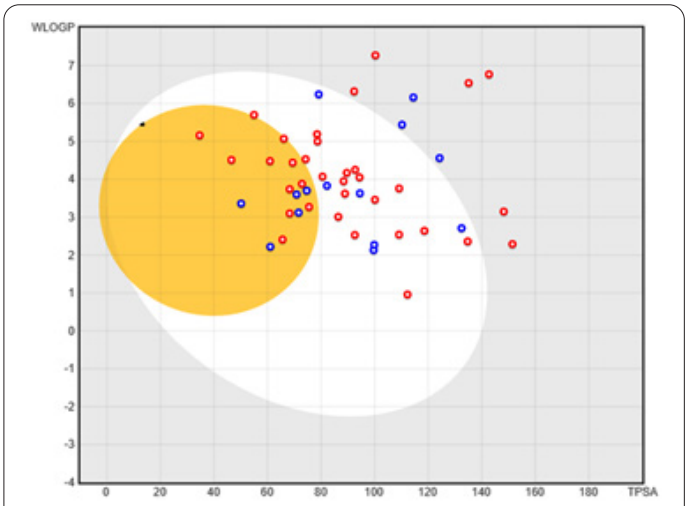


**Fig. 3.** Evaluation of ligand hits and selected inhibitors concerning passive gastrointestinal absorption (HIA) and blood-brain barrier (BBB) penetration using the BOILED-Egg model. The yellow area indicates HIA, while the white area represents BBB permeation. Ligand hits are shown as blue dots if they are P-glycoprotein (Pgp) positive and red dots if they are Pgp negative.

**Table 1.** Physicochemical attributes of ligand hits filtered via the BOILED-Egg model and established inhibitors.

| S.No | Ligands | #Physiochemical Properties | | | | | |
|---|---|---|---|---|---|---|---|
| | | MW (g/mol) | RB | HBA | HBD | TPSA (Å²) | MR |
| 1 | Mcule-2973506626 | 380.44 | 0 | 2 | 2 | 50.16 | 121.28 |
| 2 | Mcule-5816723133 | 377.82 | 3 | 4 | 4 | 54.96 | 106.84 |
| 3 | Mcule-9233397999 | 298.30 | 0 | 4 | 4 | 74.63 | 83.47 |
| 4 | Mcule-1579910267 | 344.19 | 2 | 3 | 3 | 46.5 | 91.78 |
| 5 | Mcule-8114411145 | 322.38 | 1 | 3 | 3 | 78.68 | 95.26 |
| 6 | Mcule-1991062471 | 462.01 | 6 | 3 | 3 | 79.12 | 144.83 |
| 7 | Mcule-8617639093 | 408.39 | 3 | 6 | 6 | 66.07 | 103.13 |
| 8 | Mcule-9536445798 | 491.38 | 9 | 3 | 3 | 78.51 | 131.12 |
| 9 | Mcule-4933708772 | 431.47 | 3 | 5 | 5 | 151.47 | 127.26 |
| 10 | Mcule-9992566928 | 361.37 | 4 | 5 | 5 | 60.92 | 100.1 |
| 11 | Mcule-3223214310 | 388.48 | 4 | 6 | 6 | 94.49 | 103.7 |
| 12 | Mcule-2097380359 | 424.43 | 6 | 5 | 5 | 94.35 | 122.23 |
| 13 | Mcule-1024981469 | 474.43 | 6 | 8 | 8 | 86.43 | 120.21 |
| 14 | Mcule-1893218381 | 342.28 | 3 | 8 | 8 | 69.38 | 82.69 |
| 15 | Mcule-2449737562 | 311.23 | 0 | 6 | 6 | 34.62 | 70.7 |
| 16 | Mcule-2991653790 | 441.57 | 4 | 2 | 2 | 114.45 | 130.59 |
| 17 | Mcule-4537745040 | 476.58 | 5 | 7 | 7 | 82.18 | 136.44 |
| 18 | Mcule-2225687401 | 347.44 | 2 | 3 | 3 | 71.62 | 105.96 |
| 19 | Mcule-6893679909 | 416.92 | 7 | 3 | 3 | 92.73 | 113.37 |
| 20 | Mcule-7244896358 | 478.58 | 7 | 4 | 4 | 135.11 | 131.54 |
| 21 | Mcule-4185234246 | 383.47 | 3 | 3 | 3 | 74.22 | 126.96 |
| 22 | Mcule-7907634139 | 393.82 | 2 | 4 | 4 | 88.92 | 115.24 |
| 23 | Mcule-7791872451 | 292.29 | 1 | 4 | 4 | 68.26 | 83.22 |
| 24 | Mcule-3981378344 | 331.37 | 3 | 4 | 4 | 65.6 | 96.6 |
| 25 | Mcule-5486633936 | 397.45 | 7 | 6 | 6 | 109.15 | 105.22 |
| 26 | Mcule-1058769814 | 357.47 | 4 | 5 | 5 | 61.03 | 107 |
| 27 | Mcule-4562900743 | 320.41 | 2 | 2 | 2 | 72.86 | 102.88 |
| 28 | Mcule-7790094729 | 280.32 | 2 | 2 | 2 | 68.26 | 86.36 |
| 29 | Mcule-2525256456 | 426.88 | 5 | 5 | 5 | 100.11 | 116.91 |
| 30 | Mcule-2363150472 | 432.93 | 3 | 4 | 4 | 110.23 | 122.11 |
| 31 | Mcule-7595714167 | 498.55 | 5 | 7 | 7 | 148.24 | 132.13 |
| 32 | Mcule-3430403539 | 356.37 | 4 | 5 | 5 | 118.58 | 90.8 |
| 33 | Mcule-3445614275 | 465.72 | 7 | 6 | 6 | 89.61 | 117.24 |
| 34 | Mcule-3838220036 | 440.56 | 7 | 6 | 6 | 92.6 | 127.02 |
| 35 | Mcule-7046491392 | 460.57 | 6 | 5 | 5 | 70.84 | 141.06 |
| 36 | Mcule-3034040298 | 354.40 | 5 | 5 | 5 | 80.55 | 94.02 |
| 37 | Mcule-1656232882 | 386.44 | 4 | 4 | 4 | 99.63 | 108.21 |
| 38 | Doxazosin | 451.48 | 5 | 7 | 1 | 112.27 | 128.58 |
| 39 | Dasatinib | 488.01 | 8 | 6 | 3 | 134.75 | 138.63 |
| 40 | Vemurafenib | 489.92 | 7 | 6 | 2 | 100.3 | 124.21 |
| 41 | Wortmannin | 428.43 | 4 | 8 | 0 | 109.11 | 105.71 |
| 42 | Sorafenib | 464.82 | 9 | 7 | 3 | 92.35 | 112.48 |

#.MW stands for molecular weight, RB for rotational bonds, TPSA for topological polar surface area, MR for molecular refractivity, HBA for hydrogen bond acceptor, and HBD for hydrogen bond donor.

ry and renal pathways, brain permeability, tissue accumulation, bioavailability, and toxicity. This characteristic can be quantified using the partition coefficient (Log Po/w), which is mathematically defined as follows: Log Po/w = log [ligand molecule] octanol / [ligand molecule] water. Log P is often used to determine blood-brain partitioning and is a useful indicator of the hydrophilic or hydrophobic nature of a molecule. The range of Log P values is quite extensive, spanning from +0.71 to +7.27 [50, 56]. Doxazosin exhibited the lowest Log P value of +0.71, while vemurafenib displayed the highest Log P value of +7.27 (Table 2). Fortunately, most of the selected compounds have favorable cell penetration and oral absorption properties.

### *3.2.4. Solubility*

Solubility refers to the maximum concentration of a substance that can be dissolved in a specific solvent under specific conditions. It plays a critical role in determining the intestinal absorption and oral bioavailability. Low solubility can hinder absorption and lead to reduced oral bioavailability. Solubility and permeability exhibit distinct molecular properties. Improving solubility can enhance absorption and oral bioavailability, making this a vital aspect of drug development. This is because solubility influences the rate of drug absorption into the bloodstream and the amount of drug available for bodily use.

Increasing solubility facilitates faster and more concentrated drug absorption, resulting in increased bioavailability and improved drug efficacy. SwissADME predicts the water solubility of small molecules using the log S scale, which employs three descriptors derived from the ESOL model by Ali et al. (2012) and SILICOS-IT filter [57]. The optimal water solubility ranges were classified

**Table 2.** Lipophilicity calculations for established inhibitors and BOILED-Egg model filtered ligand hits.

| S.No. | Ligands | Lipophilicity | | | | |
|---|---|---|---|---|---|---|
| | | I Log P | X Log P | W Log P | M Log P | Consensus Log P |
| 1 | Mcule-2973506626 | 3.18 | 4.47 | 3.36 | 3.88 | 3.69 |
| 2 | Mcule-5816723133 | 3.81 | 5.26 | 5.7 | 3.25 | 4.78 |
| 3 | Mcule-9233397999 | 2.59 | 3.00 | 3.7 | 1.72 | 2.81 |
| 4 | Mcule-1579910267 | 3.10 | 5.21 | 4.51 | 3.36 | 4.37 |
| 5 | Mcule-8114411145 | 3.08 | 5.50 | 5.00 | 3.56 | 4.66 |
| 6 | Mcule-1991062471 | 3.77 | 6.23 | 6.24 | 4.24 | 5.67 |
| 7 | Mcule-8617639093 | 3.02 | 3.07 | 5.07 | 3.54 | 3.55 |
| 8 | Mcule-9536445798 | 3.69 | 5.94 | 5.19 | 3.51 | 4.78 |
| 9 | Mcule-4933708772 | 1.69 | 2.79 | 2.29 | 0.75 | 2.55 |
| 10 | Mcule-9992566928 | 3.56 | 3.55 | 4.48 | 3.46 | 3.95 |
| 11 | Mcule-3223214310 | 2.57 | 2.63 | 3.63 | 1.58 | 2.37 |
| 12 | Mcule-2097380359 | 2.46 | 4.35 | 4.05 | 2.97 | 3.75 |
| 13 | Mcule-1024981469 | 3.84 | 3.26 | 3.01 | 2.67 | 3.23 |
| 14 | Mcule-1893218381 | 3.08 | 4.31 | 4.44 | 3.05 | 3.54 |
| 15 | Mcule-2449737562 | 2.52 | 4.10 | 5.16 | 4.38 | 4.21 |
| 16 | Mcule-2991653790 | 3.89 | 5.60 | 6.16 | 4.57 | 5.27 |
| 17 | Mcule-4537745040 | 3.99 | 2.80 | 3.83 | 3.36 | 3.75 |
| 18 | Mcule-2225687401 | 3.26 | 3.66 | 3.12 | 4.11 | 3.38 |
| 19 | Mcule-6893679909 | 3.77 | 4.53 | 4.25 | 2.73 | 3.94 |
| 20 | Mcule-7244896358 | 3.56 | 6.71 | 6.54 | 2.97 | 4.97 |
| 21 | Mcule-4185234246 | 3.66 | 5.74 | 4.53 | 3.76 | 4.89 |
| 22 | Mcule-7907634139 | 2.66 | 3.34 | 3.62 | 1.63 | 3.03 |
| 23 | Mcule-7791872451 | 2.62 | 3.19 | 3.10 | 2.93 | 2.96 |
| 24 | Mcule-3981378344 | 2.79 | 2.13 | 2.41 | 1.58 | 2.34 |
| 25 | Mcule-5486633936 | 2.63 | 3.48 | 3.76 | 1.37 | 2.80 |
| 26 | Mcule-1058769814 | 2.98 | 2.31 | 2.22 | 2.55 | 2.30 |
| 27 | Mcule-4562900743 | 3.06 | 4.91 | 3.88 | 4.11 | 4.28 |
| 28 | Mcule-7790094729 | 2.7 | 3.43 | 3.74 | 2.65 | 3.20 |
| 29 | Mcule-2525256456 | 2.82 | 4.31 | 3.46 | 2.5 | 3.18 |
| 30 | Mcule-2363150472 | 4.05 | 4.38 | 5.44 | 3.57 | 4.56 |
| 31 | Mcule-7595714167 | 3.09 | 2.85 | 3.15 | 2.61 | 3.04 |
| 32 | Mcule-3430403539 | 2.71 | 3.68 | 2.64 | 2.2 | 3.02 |
| 33 | Mcule-3445614275 | 3.51 | 4.83 | 4.17 | 3.12 | 4.25 |
| 34 | Mcule-3838220036 | 3.22 | 3.29 | 2.53 | 2.79 | 2.68 |
| 35 | Mcule-7046491392 | 4.69 | 5.01 | 3.60 | 2.16 | 3.92 |
| 36 | Mcule-3034040298 | 3.27 | 4.18 | 4.07 | 3.32 | 3.91 |
| 37 | Mcule-1656232882 | 2.75 | 1.97 | 2.13 | 2.38 | 2.37 |
| 38 | Doxazosin | 3.5 | 3.30 | 0.96 | 0.71 | 1.97 |
| 39 | Dasatinib | 3.37 | 3.59 | 2.36 | 1.35 | 2.8 |
| 40 | Vemurafenib | 3.04 | 4.97 | 7.27 | 3.14 | 4.84 |
| 41 | Wortmannin | 2.7 | 1.18 | 2.54 | 0.94 | 2.20 |
| 42 | Sorafenib | 3.45 | 4.07 | 6.32 | 2.91 | 4.11 |

as insoluble (10), weakly (6), moderately (4), soluble (2), extremely (0), and highly (0) soluble. Based on the computed water solubility values, ligands and inhibitors can be classified as soluble, moderately soluble, or poorly soluble, as shown in Table 3.

### *3.2.5. Pharmacokinetics Properties*

Compounds that target the central nervous system must effectively traverse the blood-brain barrier (BBB) to achieve their intended effects. The permeability of the BBB serves as a gauge of a drug's preference for blood or brain tissue, and successful BBB passage is crucial for these drugs to avoid adverse effects on the central nervous system. The majority of the compounds demonstrated high gastrointestinal absorption (GIA), suggesting their potential for easy traversal through the gut lining. The logarithmic Kp (Log Kp) values for all compounds range between -8.08 and -4.36 cm/s (Table 4). A more negative Log Kp indicates reduced skin permeability for molecules [58,59]. Consequently, these compounds have the potential to pass through the intestinal barrier effectively.

### *3.2.6. Drug-likeness prediction and evaluating medicinal chemistry attributes*

Often, the term "drug-likeness" refers to a qualitative assessment of a molecule's likelihood of possessing specific molecular and structural attributes that are similar to those of established medications. The prediction of drug-likeness was facilitated using online tools from SwissADME, which employs a diverse set of filters and five distinct criteria rooted in pharmaceutical and biotechnological principles to qualitatively anticipate the potential of a molecule as an oral drug candidate concerning bioavailability. These criteria encompass Lipinski, Veber, Egan, and Muegge rules. The majority of compounds exhibited drug-like characteristics with no violations, whereas a portion displayed one or two violations, as indicated in Table 5. The identification of potentially problematic fragments typically employs two complementary pattern recognition methods: Pan Assay Interference Compounds

**Table 3.** The computed solubility values for established inhibitors and BOILED-Egg filtered compounds.

| S.No. | Ligands | Log *S* (ESOL) | Log *S* (Ali) | Log *S* (SILICOS-IT) |
|---|---|---|---|---|
| 1 | Mcule-2973506626 | -5.55 | -5.24 | -8.03 |
| 2 | Mcule-5816723133 | -5.9 | -6.16 | -8.9 |
| 3 | Mcule-9233397999 | -4.13 | -4.23 | -5.73 |
| 4 | Mcule-1579910267 | -5.51 | -5.93 | -7.45 |
| 5 | Mcule-8114411145 | -5.85 | -6.91 | -7.25 |
| 6 | Mcule-1991062471 | -6.65 | -7.68 | -10.48 |
| 7 | Mcule-8617639093 | -4.43 | -4.12 | -5.62 |
| 8 | Mcule-9536445798 | -6.52 | -7.36 | -10.08 |
| 9 | Mcule-4933708772 | -4.62 | -5.63 | -7.92 |
| 10 | Mcule-9992566928 | -4.68 | -4.51 | -8.15 |
| 11 | Mcule-3223214310 | -3.94 | -4.26 | -4.76 |
| 12 | Mcule-2097380359 | -5.23 | -6.05 | -8.7 |
| 13 | Mcule-1024981469 | -4.83 | -4.75 | -6.14 |
| 14 | Mcule-1893218381 | -5.1 | -5.48 | -6.48 |
| 15 | Mcule-2449737562 | -4.79 | -4.53 | -5.88 |
| 16 | Mcule-2991653790 | -6.49 | -7.77 | -9.25 |
| 17 | Mcule-4537745040 | -4.5 | -4.18 | -8.49 |
| 18 | Mcule-2225687401 | -4.73 | -4.85 | -6.05 |
| 19 | Mcule-6893679909 | -5.13 | -6.2 | -7.19 |
| 20 | Mcule-7244896358 | -7.09 | -9.35 | -9.14 |
| 21 | Mcule-4185234246 | -6.19 | -7.07 | -9.11 |
| 22 | Mcule-7907634139 | -4.65 | -4.88 | -6.02 |
| 23 | Mcule-7791872451 | -4.23 | -4.29 | -5.62 |
| 24 | Mcule-3981378344 | -3.66 | -3.14 | -6.24 |
| 25 | Mcule-5486633936 | -4.48 | -5.45 | -7.41 |
| 26 | Mcule-1058769814 | -3.6 | -3.23 | -5.46 |
| 27 | Mcule-4562900743 | -5.33 | -6.18 | -6.9 |
| 28 | Mcule-7790094729 | -4.17 | -4.54 | -6.59 |
| 29 | Mcule-2525256456 | -5.33 | -6.13 | -7.54 |
| 30 | Mcule-2363150472 | -5.73 | -6.41 | -8.71 |
| 31 | Mcule-7595714167 | -4.85 | -5.62 | -7.07 |
| 32 | Mcule-3430403539 | -4.61 | -5.86 | -5.34 |
| 33 | Mcule-3445614275 | -5.73 | -6.45 | -8.79 |
| 34 | Mcule-3838220036 | -4.59 | -4.91 | -5.92 |
| 35 | Mcule-7046491392 | -5.78 | -6.24 | -7.66 |
| 36 | Mcule-3034040298 | -4.93 | -5.58 | -6.82 |
| 37 | Mcule-1656232882 | -3.54 | -3.69 | -5.85 |
| 38 | Doxazosin | 2.37 | -5.33 | -5.15 |
| 39 | Dasatinib | -4.98 | -6.11 | -6.88 |
| 40 | Vemurafenib | -6.02 | -6.81 | -10.07 |
| 41 | Wortmannin | -3.1 | -3.07 | -5.15 |
| 42 | Sorafenib | -5.11 | -5.71 | -8.6 |

(PAINS) and Brenk filter. PAINS, also known as promiscuous compounds, contains substructures that yield misleading responses in biologically active assays, irrespective of the protein receptor. The Brenk filter serves as a structural alarm, warning about chemically reactive, metabolically unstable fragments within the structure that could lead to unfavorable pharmacokinetics. As outlined in Table 5, most compounds triggered no alerts, although Mcule-1579910267 raised flags for 01 Brenk and 02 PAINS. Through the application of the PAINS and Brenk filters, it became apparent that the majority of compounds adhered to the lead-likeness criteria. During lead optimization, compounds typically undergo chemical modifications that often increase their size and lipophilicity [60]. Most compounds demonstrated zero violations, indicating their suitability for lead optimization, whereas a subset displayed one or two violations. Synthetic Accessibility (SA) scores for all compounds were below 0.5, with the exception of Mcule-4537745040 and Wortmannin, which surpassed this threshold. The SA score was normalized within the range of 1–10 (Table 5).

### 3.3. Molecular interaction studies

The molecular interactions between ADMET-filtered hits and EphA2 were investigated using three distinct tools: AutoDock Vina, DockThor, and SwissDock. The average free energy of binding was calculated to identify consistent lead compounds.

#### *3.3.1. AutoDock Vina*

Using the ADV tool developed by Mcule, we conducted docking simulations with EphA2 for all nine ligand hits (Mcule-1579910267, Mcule-1893218381, Mcule-2449737562,Mcule-3981378344,Mcule-4562900743, Mcule-7790094729,Mcule-7791872451, Mcule-8617639093, Mcule-9992566928) and reference inhibitors (Dasatinib, Vemurafenib, Wortmannin, Sorafenib) to determine their binding affinities, represented by free energy changes (ΔG). Our results revealed that doxazosin was the most potent inhibitor, with a ΔG of -8.6 kcal/mol.

Interestingly, the ligand hits exhibited significantly improved binding interactions compared with doxazosin,

**Table 4.** Calculated pharmacokinetics properties of known inhibitors and BOILED-Egg filtered ligand hits.

| S. No. | Ligands | Drug-likeness | | | | | Medicinal Chemistry Attributes | | | | |
|---|---|---|---|---|---|---|---|---|---|---|---|
| | | Number of violation | | | | | *BAS | PAINS | Brenk | Lead likeness | #SA |
| | | RO5 | Ghose | Veber | Egan | Muegge | | | | | |
| 1 | Mcule-2973506626 | 0 | 0 | 0 | 0 | 0 | 0.55 | 0 | 0 | 2 | 4.31 |
| 2 | Mcule-5816723133 | 0 | 1 | 0 | 0 | 0 | 0.55 | 0 | 0 | 2 | 3.52 |
| 3 | Mcule-9233397999 | 0 | 0 | 0 | 0 | 0 | 0.55 | 0 | 0 | 0 | 3.11 |
| 4 | Mcule-1579910267 | 0 | 0 | 0 | 0 | 0 | 0.55 | 2 | 1 | 1 | 3.40 |
| 5 | Mcule-8114411145 | 0 | 0 | 0 | 0 | 0 | 0.55 | 0 | 0 | 1 | 3.46 |
| 6 | Mcule-1991062471 | 1 | 0 | 0 | 1 | 0 | 0.55 | 0 | 0 | 2 | 4.2 |
| 7 | Mcule-8617639093 | 0 | 0 | 0 | 0 | 0 | 0.55 | 1 | 0 | 1 | 3.73 |
| 8 | Mcule-9536445798 | 0 | 0 | 0 | 0 | 0 | 0.55 | 0 | 2 | 3 | 3.38 |
| 9 | Mcule-4933708772 | 0 | 0 | 0 | 1 | 0 | 0.55 | 0 | 0 | 1 | 4.37 |
| 10 | Mcule-9992566928 | 0 | 0 | 0 | 0 | 0 | 0.55 | 0 | 0 | 2 | 3.35 |
| 11 | Mcule-3223214310 | 0 | 0 | 0 | 0 | 0 | 0.55 | 0 | 0 | 1 | 4.51 |
| 12 | Mcule-2097380359 | 0 | 0 | 0 | 0 | 0 | 0.55 | 0 | 2 | 2 | 3.86 |
| 13 | Mcule-1024981469 | 0 | 0 | 0 | 0 | 0 | 0.55 | 0 | 0 | 1 | 3.55 |
| 14 | Mcule-1893218381 | 0 | 0 | 0 | 0 | 0 | 0.55 | 0 | 0 | 1 | 2.83 |
| 15 | Mcule-2449737562 | 1 | 0 | 0 | 0 | 0 | 0.55 | 0 | 2 | 1 | 3.01 |
| 16 | Mcule-2991653790 | 1 | 0 | 0 | 1 | 0 | 0.55 | 0 | 0 | 2 | 3.74 |
| 17 | Mcule-4537745040 | 0 | 0 | 0 | 0 | 0 | 0.55 | 0 | 0 | 1 | 5.12 |
| 18 | Mcule-2225687401 | 0 | 0 | 0 | 0 | 0 | 0.55 | 0 | 0 | 1 | 3.11 |
| 19 | Mcule-6893679909 | 0 | 0 | 0 | 0 | 0 | 0.55 | 0 | 0 | 2 | 4.08 |
| 20 | Mcule-7244896358 | 0 | 2 | 0 | 0 | 0 | 0.55 | 0 | 0 | 2 | 4.1 |
| 21 | Mcule-4185234246 | 0 | 0 | 0 | 0 | 0 | 0.55 | 0 | 0 | 2 | 3.95 |
| 22 | Mcule-7907634139 | 0 | 0 | 0 | 0 | 0 | 0.55 | 0 | 0 | 1 | 4.21 |
| 23 | Mcule-7791872451 | 0 | 0 | 0 | 0 | 0 | 0.55 | 0 | 0 | 0 | 3.25 |
| 24 | Mcule-3981378344 | 0 | 0 | 0 | 0 | 0 | 0.55 | 0 | 0 | 0 | 2.98 |
| 25 | Mcule-5486633936 | 0 | 0 | 0 | 0 | 0 | 0.55 | 0 | 1 | 1 | 3.72 |
| 26 | Mcule-1058769814 | 0 | 0 | 0 | 0 | 0 | 0.55 | 0 | 0 | 1 | 3.56 |
| 27 | Mcule-4562900743 | 0 | 0 | 0 | 0 | 0 | 0.55 | 0 | 0 | 1 | 4.11 |
| 28 | Mcule-7790094729 | 0 | 0 | 0 | 0 | 0 | 0.55 | 0 | 0 | 0 | 3.4 |
| 29 | Mcule-2525256456 | 0 | 0 | 0 | 0 | 0 | 0.55 | 0 | 0 | 2 | 3.92 |
| 30 | Mcule-2363150472 | 0 | 0 | 0 | 0 | 0 | 0.55 | 0 | 0 | 2 | 3.81 |
| 31 | Mcule-7595714167 | 0 | 0 | 0 | 0 | 0 | 0.55 | 0 | 0 | 1 | 3.7 |
| 32 | Mcule-3430403539 | 0 | 0 | 0 | 0 | 0 | 0.55 | 0 | 0 | 2 | 3.48 |
| 33 | Mcule-3445614275 | 0 | 0 | 0 | 0 | 0 | 0.55 | 0 | 0 | 2 | 4.11 |
| 34 | Mcule-3838220036 | 0 | 0 | 0 | 0 | 0 | 0.55 | 0 | 0 | 1 | 4.42 |
| 35 | Mcule-7046491392 | 0 | 0 | 0 | 0 | 0 | 0.55 | 2 | 0 | 2 | 4.86 |
| 36 | Mcule-3034040298 | 0 | 0 | 0 | 0 | 0 | 0.55 | 0 | 0 | 2 | 3.39 |
| 37 | Mcule-1656232882 | 0 | 0 | 0 | 0 | 0 | 0.55 | 0 | 0 | 1 | 3.67 |
| 38 | Doxazosin | 0 | 0 | 0 | 0 | 0 | 0.55 | 0 | 0 | 1 | 4.03 |
| 39 | Dasatinib | 0 | 2 | 0 | 1 | 0 | 0.55 | 0 | 0 | 3 | 3.83 |
| 40 | Vemurafenib | 0 | 2 | 0 | 1 | 0 | 0.55 | 0 | 0 | 2 | 3.38 |
| 41 | Wortmannin | 0 | 0 | 0 | 0 | 0 | 0.55 | 0 | 1 | 2 | 4.92 |
| 42 | Sorafenib | 0 | 1 | 0 | 1 | 0 | 0.55 | 0 | 1 | 1 | 5.66 |

as detailed in Table 6. Specifically, Mcule-1579910267 (ΔG: -10.8 kcal/mol), Mcule-1893218381 (ΔG: -10.4 kcal/mol), Mcule-2449737562 (ΔG: -10.4 kcal/mol), Mcule-3981378344 (ΔG: -9.8 kcal/mol), Mcule-4562900743 (ΔG: -9.7 kcal/mol), Mcule-7790094729 (ΔG: -9.7 kcal/mol), Mcule-7791872451 (ΔG: -9.9 kcal/mol), Mcule-8617639093 (ΔG: -10.7 kcal/mol), and Mcule-9992566928 (ΔG: -10.5 kcal/mol) demonstrated notably improved binding affinities (Table 6).

To validate the consistency of their binding patterns, we conducted docking simulations with EphA2 using two distinct tools, DockThor and SwissDock. This approach aimed to ascertain the reliability and robustness of observed interactions. Further investigation and analysis of these promising ligand hits could offer valuable insights into their potential as effective EphA2 inhibitors, potentially surpassing the efficacy of doxazosin.

### *3.3.2. DockThor*

DockThor predicted Dasatinib to be a more potent binder with EphA2 than Doxazosin (ΔG: -8.3 kcal/mol), showing a binding energy of ΔG: -9.1 kcal/mol. Among the ligand hits, seven compounds, namely Mcule-1579910267 (ΔG: -10.0 kcal/mol), Mcule-1893218381 (ΔG: -9.4 kcal/mol), Mcule-2449737562 (ΔG: -9.6 kcal/mol), Mcule-3981378344 (ΔG: -9.4 kcal/mol), Mcule-7790094729 (ΔG: -9.4 kcal/mol), Mcule-7791872451 (ΔG: -9.2 kcal/mol), and Mcule-9992566928 (ΔG: -9.6 kcal/mol), demonstrated a higher binding affinity compared to Dasatinib. However, molecules Mcule-4562900743 (ΔG: -9.1 kcal/mol) and Mcule-8617639093 (ΔG: -7.9 kcal/mol) exhibited similar and weaker binding interactions with EphA2 compared to Dasatinib (Table 6).

**Table 5.** Calculated drug-likeness and medicinal chemistry properties of known inhibitors and BOILED-Egg filtered ligand hits.

| S. No. | Ligands | Drug-likeness | | | | | Medicinal Chemistry Attributes | | | | |
|---|---|---|---|---|---|---|---|---|---|---|---|
| | | Number of violation | | | | | *BAS | PAINS | Brenk | Lead likeness | #SA |
| | | RO5 | Ghose | Veber | Egan | Muegge | | | | | |
| 1 | Mcule-2973506626 | 0 | 0 | 0 | 0 | 0 | 0.55 | 0 | 0 | 2 | 4.31 |
| 2 | Mcule-5816723133 | 0 | 1 | 0 | 0 | 0 | 0.55 | 0 | 0 | 2 | 3.52 |
| 3 | Mcule-9233397999 | 0 | 0 | 0 | 0 | 0 | 0.55 | 0 | 0 | 0 | 3.11 |
| 4 | Mcule-1579910267 | 0 | 0 | 0 | 0 | 0 | 0.55 | 2 | 1 | 1 | 3.40 |
| 5 | Mcule-8114411145 | 0 | 0 | 0 | 0 | 0 | 0.55 | 0 | 0 | 1 | 3.46 |
| 6 | Mcule-1991062471 | 1 | 0 | 0 | 1 | 0 | 0.55 | 0 | 0 | 2 | 4.2 |
| 7 | Mcule-8617639093 | 0 | 0 | 0 | 0 | 0 | 0.55 | 1 | 0 | 1 | 3.73 |
| 8 | Mcule-9536445798 | 0 | 0 | 0 | 0 | 0 | 0.55 | 0 | 2 | 3 | 3.38 |
| 9 | Mcule-4933708772 | 0 | 0 | 0 | 1 | 0 | 0.55 | 0 | 0 | 1 | 4.37 |
| 10 | Mcule-9992566928 | 0 | 0 | 0 | 0 | 0 | 0.55 | 0 | 0 | 2 | 3.35 |
| 11 | Mcule-3223214310 | 0 | 0 | 0 | 0 | 0 | 0.55 | 0 | 0 | 1 | 4.51 |
| 12 | Mcule-2097380359 | 0 | 0 | 0 | 0 | 0 | 0.55 | 0 | 2 | 2 | 3.86 |
| 13 | Mcule-1024981469 | 0 | 0 | 0 | 0 | 0 | 0.55 | 0 | 0 | 1 | 3.55 |
| 14 | Mcule-1893218381 | 0 | 0 | 0 | 0 | 0 | 0.55 | 0 | 0 | 1 | 2.83 |
| 15 | Mcule-2449737562 | 1 | 0 | 0 | 0 | 0 | 0.55 | 0 | 2 | 1 | 3.01 |
| 16 | Mcule-2991653790 | 1 | 0 | 0 | 1 | 0 | 0.55 | 0 | 0 | 2 | 3.74 |
| 17 | Mcule-4537745040 | 0 | 0 | 0 | 0 | 0 | 0.55 | 0 | 0 | 1 | 5.12 |
| 18 | Mcule-2225687401 | 0 | 0 | 0 | 0 | 0 | 0.55 | 0 | 0 | 1 | 3.11 |
| 19 | Mcule-6893679909 | 0 | 0 | 0 | 0 | 0 | 0.55 | 0 | 0 | 2 | 4.08 |
| 20 | Mcule-7244896358 | 0 | 2 | 0 | 0 | 0 | 0.55 | 0 | 0 | 2 | 4.1 |
| 21 | Mcule-4185234246 | 0 | 0 | 0 | 0 | 0 | 0.55 | 0 | 0 | 2 | 3.95 |
| 22 | Mcule-7907634139 | 0 | 0 | 0 | 0 | 0 | 0.55 | 0 | 0 | 1 | 4.21 |
| 23 | Mcule-7791872451 | 0 | 0 | 0 | 0 | 0 | 0.55 | 0 | 0 | 0 | 3.25 |
| 24 | Mcule-3981378344 | 0 | 0 | 0 | 0 | 0 | 0.55 | 0 | 0 | 0 | 2.98 |
| 25 | Mcule-5486633936 | 0 | 0 | 0 | 0 | 0 | 0.55 | 0 | 1 | 1 | 3.72 |
| 26 | Mcule-1058769814 | 0 | 0 | 0 | 0 | 0 | 0.55 | 0 | 0 | 1 | 3.56 |
| 27 | Mcule-4562900743 | 0 | 0 | 0 | 0 | 0 | 0.55 | 0 | 0 | 1 | 4.11 |
| 28 | Mcule-7790094729 | 0 | 0 | 0 | 0 | 0 | 0.55 | 0 | 0 | 0 | 3.4 |
| 29 | Mcule-2525256456 | 0 | 0 | 0 | 0 | 0 | 0.55 | 0 | 0 | 2 | 3.92 |
| 30 | Mcule-2363150472 | 0 | 0 | 0 | 0 | 0 | 0.55 | 0 | 0 | 2 | 3.81 |
| 31 | Mcule-7595714167 | 0 | 0 | 0 | 0 | 0 | 0.55 | 0 | 0 | 1 | 3.7 |
| 32 | Mcule-3430403539 | 0 | 0 | 0 | 0 | 0 | 0.55 | 0 | 0 | 2 | 3.48 |
| 33 | Mcule-3445614275 | 0 | 0 | 0 | 0 | 0 | 0.55 | 0 | 0 | 2 | 4.11 |
| 34 | Mcule-3838220036 | 0 | 0 | 0 | 0 | 0 | 0.55 | 0 | 0 | 1 | 4.42 |
| 35 | Mcule-7046491392 | 0 | 0 | 0 | 0 | 0 | 0.55 | 2 | 0 | 2 | 4.86 |
| 36 | Mcule-3034040298 | 0 | 0 | 0 | 0 | 0 | 0.55 | 0 | 0 | 2 | 3.39 |
| 37 | Mcule-1656232882 | 0 | 0 | 0 | 0 | 0 | 0.55 | 0 | 0 | 1 | 3.67 |
| 38 | Doxazosin | 0 | 0 | 0 | 0 | 0 | 0.55 | 0 | 0 | 1 | 4.03 |
| 39 | Dasatinib | 0 | 2 | 0 | 1 | 0 | 0.55 | 0 | 0 | 3 | 3.83 |
| 40 | Vemurafenib | 0 | 2 | 0 | 1 | 0 | 0.55 | 0 | 0 | 2 | 3.38 |
| 41 | Wortmannin | 0 | 0 | 0 | 0 | 0 | 0.55 | 0 | 1 | 2 | 4.92 |
| 42 | Sorafenib | 0 | 1 | 0 | 1 | 0 | 0.55 | 0 | 1 | 1 | 5.66 |

**Table 6**. Molecular interactions of the top nine ligands and reference inhibitors.

| S. No | Ligand name | AutoDock Vina | DockThor | SwissDock | *ΔG* (Average) |
|---|---|---|---|---|---|
| | | (kcal/mol) | | | |
| 1 | Mcule-1579910267 | -10.8 | -10.0 | -7.1 | -9.3 |
| 2 | Mcule-1893218381 | -10.4 | -9.4 | -7.8 | -9.2 |
| 3 | Mcule-2449737562 | -10.4 | -9.6 | -6.1 | -8.7 |
| 4 | Mcule-3981378344 | -9.8 | -9.4 | -8.8 | -9.3 |
| 5 | Mcule-4562900743 | -9.7 | -9.1 | -7.1 | -8.6 |
| 6 | Mcule-7790094729 | -9.7 | -9.4 | -8.1 | -9.0 |
| 7 | Mcule-7791872451 | -9.9 | -9.2 | -7.0 | -8.7 |
| 8 | Mcule-8617639093 | -10.7 | -7.9 | -6.9 | -9.1 |
| 9 | Mcule-9992566928 | -10.5 | -9.6 | -7.2 | -9.1 |
| 10 | Dasatinib | -7.7 | -9.1 | -8.1 | -8.3 |
| 11 | Doxazosin | -8.6 | -8.3 | -7.3 | -8.1 |
| 12 | Vemurafenib | -8.6 | -9.1 | -7.3 | -8.3 |
| 13 | Wortmannin | -8.6 | -8.1 | -6.1 | -7.6 |
| 14 | Sorafenib | -7.2 | -6.4 | -8.6 | -7.4 |

### *3.3.3. SwissDock*

SwissDock analysis revealed that the inhibitor Sorafenib, with a calculated binding free energy (ΔG) of -8.6 kcal/mol, exhibited significant interactions with the EphA2 receptor compared to the reference inhibitor Dasatinib (ΔG: -8.1 kcal/mol). A single ligand hit, namely Mcule-3981378344 (ΔG: -9.4 kcal/mol), demonstrated a stronger binding affinity than Dasatinib, while the other ligand hits displayed weak interactions with Sorafenib. To identify potential drug candidates with enhanced binding capabilities, a consensus ΔG was determined by averaging the ΔG values predicted by three selected docking methods for each compound. The conformational arrangement of molecules and their intermolecular forces significantly influence their interactions, and docking methods aid in predicting optimal ligand binding orientations within receptor binding pockets, crucial for identifying potent ligands.

The negative sign in the energy released during binding interactions signifies stronger binding. Based on calculated ΔG values, nine molecules, namely Mcule-1579910267, Mcule-1893218381,Mcule-2449737562,Mcule-3981378344,Mcule-4562900743, Mcule-7790094729, Mcule-7791872451,Mcule-8617639093,and Mcule-9992566928, displayed favorable interactions with EphA2 compared to Dasatinib. Consequently, Dasatinib and the top four hits were selected for a 50ns molecular dynamics simulation study. Docking affinities of the top nine ligands and reference inhibitors are shown in Table 6.

## 3.4. MD simulation study

Using the GROMACS software, a 50-nanosecond Molecular Dynamics Simulation (MDS) was carried out to investigate the stability of the docked complexes that included the top four hits: Mcule-1579910267, Mcule-1893218381, Mcule-3981378344, and Mcule-8617639093, as well as the known inhibitor Dasatinib, in connection with EphA2. To thoroughly evaluate the molecular interactions and stability of the complex, various plots were generated, such as the Root Mean Square Deviation (RMSD), Root Mean Square Fluctuation (RMSF), Solvent Accessible Surface Area (SASA), Free Energy of Solvation during SASA, Gyration, and Hydrogen Bonds. Binding of the ligands to the active site of EphA2 results in conformational adjustments, which contribute to the stability of the complexes [61,62].

### *3.4.1. Root mean square deviation*

Protein stability and its similarity to the native structure are typically gauged using Root Mean Square Deviation (RMSD) and Root Mean Square Fluctuation (RMSF), both of which provide valuable insights. In the case of EphA2 complexes, the RMSD values for Dasatinib (black), Mcule-3981378344 (blue), Mcule-1579910267 (red), Mcule-1893218381 (green), and Mcule-8617639093 (yellow) were 0.38 nm, 0.42 nm, 0.38 nm, 0.33 nm, and 0.34 nm, respectively. These values are presented in Figure 4A and Table 7.

The RMSD plot effectively illustrates the dynamic behavior of these complexes over time. Notably, the complex containing Mcule-1893218381 and EphA2 exhibited enhanced stability compared to the dasatinib complex. This observation indicates that Mcule-1893218381 formed a more consistent interaction with the EphA2 receptor, leading to a more stable complex throughout the simulation period.

### *3.4.2. Root mean square fluctuation*

Assessing the stability of protein-ligand complexes during molecular dynamics (MD) simulation is crucial for understanding the interactions between molecules. To achieve this, Root Mean Square Fluctuation (RMSF) was utilized to quantify the fluctuations of residues in the complex. While the Root Mean Square Deviation (RMSD) provides information about the average spatial displacement of the complex, the RMSF provides insights into the structural stability of the complex. The figure presented in the text highlights residue fluctuations during the interaction with Mcule-3981378344 and Mcule-8617639093 (Figure 4B). It is noteworthy that the figure demonstrates that the variations in residues are more pronounced during binding with Mcule-3981378344 compared to Mcule-8617639093. This observation suggests that the ligands and inhibitors had distinct effects on EphA2 throughout the simulation. The RMSF values provide information on the flexibility of specific residues within the binding pocket and shed light on the extent of the structural perturbations caused by different ligands and inhibitors. Therefore, RMSF is a valuable tool for investigating the stability of protein-ligand complexes during MD simulations.

### *3.4.3. Solvent accessible surface area and free energy of solvation*

Figure 4C presents a comprehensive examination of solvent accessibility surface area (SASA) as a method for differentiating between protein models that exhibit native-like and non-native-like behavior. This approach offers a more precise measurement of the protein surface exposure to solvent molecules, revealing intricate details that might otherwise go unnoticed. In the context of the interactions between EphA2 and the compounds Dasatinib, Mcule-3981378344, Mcule-1579910267, Mcule-1893218381, and Mcule-8617639093, the average SASA values were calculated to be 21.42 $nm^2$, 21.32 $nm^2$, 21.37 $nm^2$, 21.36 $nm^2$, and 21.27 $nm^2$, respectively. The findings in Figure 4C indicate that, when bound to EphA2, Dasatinib and Mcule-1893218381 lead to a decrease in the solvent accessibility of internal EphA2 residues compared to the binding of Mcule-8617639093. This suggests that the former compounds induce a more compact and less solvent-exposed conformation of EphA2, suggesting more stable interactions.

Further insights into the binding interactions were provided by the average free energy of solvation for each compound. Specifically, the values of ΔGSolv were determined to be -28.59 kJ/mol/$nm^2$, -28.83 kJ/mol/$nm^2$, -28.86 kJ/mol/$nm^2$, -28.74 kJ/mol/$nm^2$, and -28.82 kJ/mol/$nm^2$ for Dasatinib, Mcule-3981378344, Mcule-1579910267, Mcule-1893218381, and Mcule-8617639093, respectively (Table 7).

The combined analysis of root-mean-square deviation (RMSD), root-mean-square fluctuation (RMSF), SASA, and free energy of solvation plot strongly supports Mcule-1893218381 and Mcule-8617639093 as promising inhibitors of the target protein EphA2. These compounds exhibit favorable interactions, as inferred from their ability to induce a more constrained solvent-exposed conformation of EphA2 and the calculated free energy of solvation. This collective evidence suggests that Mcule-1893218381

and Mcule-8617639093 are potential candidates for further exploration as EphA2 inhibitors.

### *3.4.4. Radius of Gyration*

The assessment of protein compactness in biological systems involves analyzing a parameter known as the radius of gyration (Rg). The relationship between Rg and protein stability was inverse, indicating that a more compact protein exhibits a lower Rg value. In this study, we examined the average Rg values for different EphA2-compound complexes, including EphA2-Dasatinib (depicted in black), EphA2-Mcule-1579910267 (highlighted in red), EphA2-Mcule-3981378381 (represented in green), EphA2-Mcule-1893218344 (shown in blue), and EphA2-Mcule-8617639093 (indicated in yellow). The respective average Rg values were 2.044, 2.115, 2.048, 2.064, and 2.018 nm (Table 7).

During the 50ns molecular dynamics simulation, we made an interesting observation: the average Rg values for the top hit compounds and the inhibitor remained remarkably similar. Notably, the EphA2-Mcule-8617639093 complex exhibited comparatively low Rg values, indicating a more compact conformation. In contrast, EphA2-Mcule-1579910267 displayed a relatively high Rg value, suggesting a relatively less compact structure (Figure 4D). Our analysis highlights the interplay between protein compactness and stability, providing valuable insights into the behavior of these compounds when interacting with EphA2.

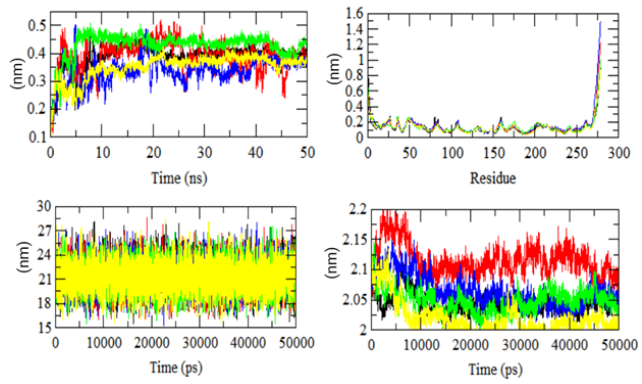


**Fig. 4. A-D.** Dynamics metrics of selected EphA2-ligand complexes. A) RMSD tracks stability and conformational changes. B) RMSF shows residue-specific fluctuations. C) SASA indicates solvent exposure. D) Rg illustrates protein compactness changes over time. Complexes analyzed: EphA2-Dasatinib (black), EphA2-Mcule-1579910267 (red), EphA2-Mcule-3981378381 (green), EphA2-Mcule-1893218344 (blue), and EphA2-Mcule-8617639093 (yellow).

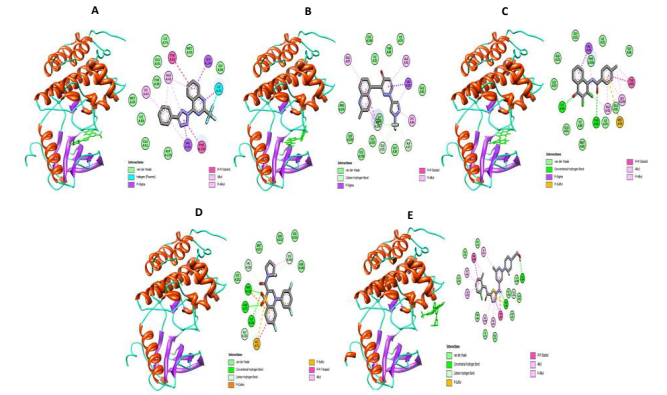


**Fig. 5. A-E.** Molecular interaction of selected ligands and EphA2. A) Mcule-3981378381, B) Mcule-1893218344, C) Mcule-1579910267, D) Mcule-8617639093, and E) Dasatinib. In each panel, a 3D representation shows the EphA2-ligand complex, with ligands depicted in brown sticks firmly attached within the EphA2 cleft. The binding residues on EphA2 are illustrated in a 2D format, with a color legend indicating bond type and amino acid residues denoted by their three-letter codes.

In comparison to Doxazosin and Dasatinib, our screening process identified nine ligands with robust binding interactions to EphA2, based on average Gibbs free energy (Table 6). Among these, the EphA2-Mcule-3981378381 and EphA2-Mcule-1893218344 complexes were notably stable, engaging in six distinct types of interactions: Mcule-3981378381 exhibited van der Waals, halogen (fluorine), pi-sigma, pi-pi stacked, alkyl, and pi-alkyl interactions. Notably, all four rings of EphA2-Mcule-3981378381 established chemical interactions with sixteen residues of EphA2 (TYR92, ILE74, ALA42, GLU91, THR90, LYS44, MET65, ILE88, GLU61, ASP155, VAL29, PHE156, ILE21, GLY96, LEU144, and MET93) (Figure 5A).

Similarly, in the EphA2-Mcule-1893218344 complex, six distinct chemical interactions - van der Waals, carbon-hydrogen bond, unfavorable donor-donor, pi-sigma, pi-pi stacked, and pi-alkyl - were observed. This complex engaged with eighteen residues of EphA2 (ALA97, ARG141, SER159, LEU158, GLY157, PHE156, GLY22, GLU25, GLU24, ALA23, LYS44, GLU61, VAL29, ALA42, ILE74, THR90, ILE21, and LEU144) (Figure 5B).

The EphA2-Mcule-1579910267 complex displayed seven types of chemical interactions - van der Waals, conventional hydrogen bond, pi-sigma, pi-sulfur, pi-pi stacked, alkyl, and pi-alkyl. All four rings of EphA2-Mcule-1579910267 contributed to chemical interactions with eighteen residues of EphA2 (LYS44, GLU61, ILE88,

**Table 7.** Summary of calculated molecular dynamics simulation parameters.

| Ligands | Average PE (kJ/mol) | Average RMSD (nm) | Average SASA ($nm^2$) | ΔGsolv ($kJ/mol/nm^2$) | Rg (nm) | Volume ($nm^3$) | Density ($kg/m^3$) |
|---|---|---|---|---|---|---|---|
| Mcule-1579910267 | -935512 | 0.387 | 21.37 | -28.86 | 2.1154 | 702.197 | 1024.87 |
| Mcule-3981378344 | -935053 | 0.337 | 21.36 | -28.74 | 2.0640 | 702.104 | 1024.79 |
| Mcule-1893218381 | -935639 | 0.429 | 21.31 | -28.83 | 2.0485 | 702.155 | 1024.76 |
| Mcule-8617639093 | -935990 | 0.349 | 21.27 | -28.82 | 2.0189 | 702.321 | 1024.83 |
| Dasatinib | -937051 | 0.385 | 21.42 | -28.58 | 2.0440 | 702.167 | 1024.74 |

MET65, THR90, ILE74, ALA42, GLU91, MET93, LUE144, TYS92, GLY96, ILE21, GLY96, VAL29, PHE156, GLY22 and ALA23) (Figure 5C).

In the case of the EphA2-Mcule-8617639093 complex, eight distinct chemical bonds were observed - van der Waals, conventional hydrogen bond, carbon-hydrogen bond, unfavorable positive-positive, pi-cation, pi-sulfur, pi-pi T shaped, and alkyl. These interactions engaged twelve chemical interactions with nineteen residues of EphA2 (ASN148, LEU149, LEU112, GLN113, MET117, VAL150, CYS151, ARG119, ASN72, GLY116, GLY120, and HIS71) (Figure 5D). Finally, the molecular interaction pattern of the EphA2-Dasatinib complex exhibited eight types of binding interactions: van der Waals, conventional hydrogen bond, carbon-hydrogen bond, halogen (fluorine), unfavorable donor-donor, pi-cation, pi-donor hydrogen bond, and alkyl. All five rings of Dasatinib were found to engage in chemical interactions with nine residues of EphA2 (ARG141, SER159, ASP99, ARG103, LYS161, ARG199, ARG165, ASN206, and SER205) (Figure 5E).

The analysis showcases the diverse and intricate nature of chemical interactions within the various EphA2-ligand complexes. The specific binding interactions and residues involved offer insights into the structural basis of the ligand-protein interactions, enhancing our understanding of their potential for targeted therapeutic applications.

### *3.4.5. Hydrogen bonds analysis*

Hydrogen bonding is a crucial factor in the molecular recognition process and is essential for specifying the interactions between proteins and ligands. Molecular Dynamics (MD) simulations provided valuable information about these interactions over time, as demonstrated by the analysis of compounds EphA2-Dasatinib, EphA2-Mcule-1579910267, EphA2-Mcule-3981378381, EphA2-Mcule-1893218344, and EphA2-Mcule-8617639093.

During a 50 ns MD simulation, the formation and dynamics of hydrogen bonds between these ligands and the EphA2 protein were evaluated. Hydrogen bonds are formed when a hydrogen atom is shared between a hydrogen bond donor (e.g., an electronegative atom with a hydrogen atom) and a hydrogen bond acceptor (e.g., an electronegative atom with a lone pair of electrons). Although relatively weak compared to covalent bonds, hydrogen bonds are indispensable for molecular interactions because of their specificity and versatility.

The analysis revealed varying numbers of hydrogen bonds formed between the ligands and EphA2, ranging from 1 to 5 bonds. Specifically, Dasatinib exhibited 3-4 hydrogen bonds, Mcule-1579910267 showed 1-2 bonds, Mcule-3981378381 demonstrated 1-5 bonds, Mcule-1893218344 displayed 1-4 bonds, and Mcule-8617639093 had 2-3 bonds with the EphA2 protein (Figure 6A-E).

The observed hydrogen-bonding patterns emphasize the significance of these interactions in molecular recognition. Hydrogen bonds contribute to the specificity of these interactions, ensuring that the ligands are selectively recognized. Furthermore, multiple hydrogen bonds collectively contribute to the stability of protein-ligand complexes, preventing premature dissociation. The direct correlation between the number of hydrogen bonds and binding affinity highlights their role in modulating interaction strength.

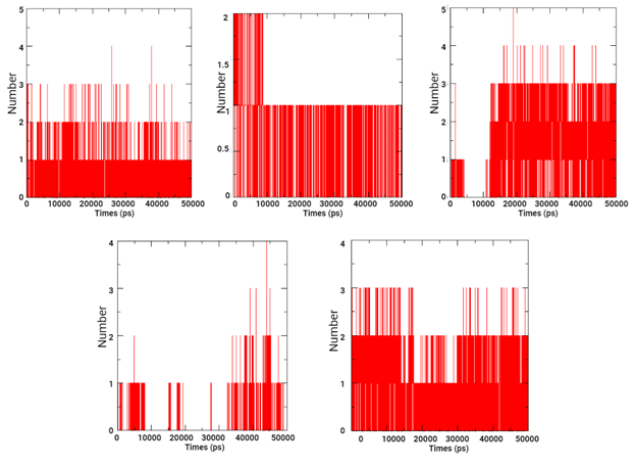


**Fig. 6. A-E.** Hydrogen Bond Dynamics plots for interactions between EphA2 and selected compounds. A) Shows H-Bond Formation and Deformation in Dasatinib-EphA2 Interaction. B) Reveals H-Bond Formation and Disruption for Mcule-1579910267 with EphA2. C) Visualizes H-Bond Dynamics during Mcule-1893218344 interaction with EphA2. D) Represents Hydrogen Bonding Patterns for Mcule-3981378381 with EphA2. E) Illustrates H-Bond Establishment and Dissolution for Mcule-8617639093 with EphA2.

In addition, hydrogen-bonding-induced conformational changes were evident, aligning the ligands optimally within EphA2's binding pocket. The MD simulation captured the dynamic fluctuations in hydrogen bond formation, offering insights into the transient nature of these interactions.

Over the course of a 50 ns Molecular Dynamics (MD) simulation, an analysis of the Root Mean Square Deviation (RMSD) was conducted for the EphA2 protein backbone, the ligand hits, the reference inhibitor, and their respective complexes. This analysis revealed intriguing insights into the stability of these molecular systems upon binding interactions.

Remarkably, the ligand Mcule-1579910267 exhibited a notably higher stability upon binding to EphA2, when compared to Dasatinib and the other ligands. The RMSD analysis indicated that Mcule-1579910267 complexed with EphA2 displayed minimal deviation from its initial conformation, suggesting a robust and relatively stable interaction.

Conversely, upon binding, deviations were observed in the complexes involving Mcule-3981378381, Mcule-1893218344, and Mcule-8617639093. These ligands demonstrated varying degrees of structural deviation from their initial conformations during the simulation. This could be indicative of more dynamic interactions or less optimal binding geometries, resulting in increased conformational flexibility,

provides a visual representation of these observations. The RMSD plots depict the changes in structural alignment of the EphA2 backbone, ligands, reference inhibitor, and their respective complexes over the simulation duration. Peaks in the RMSD curves signify periods of increased structural deviation, suggesting fluctuations in the binding interactions Figure 7 (A-E).

Overall, the RMSD analysis underscores Mcule-1579910267's enhanced stability upon binding to EphA2 in contrast to other ligands like Dasatinib and Mcule-3981378381, Mcule-1893218344, and

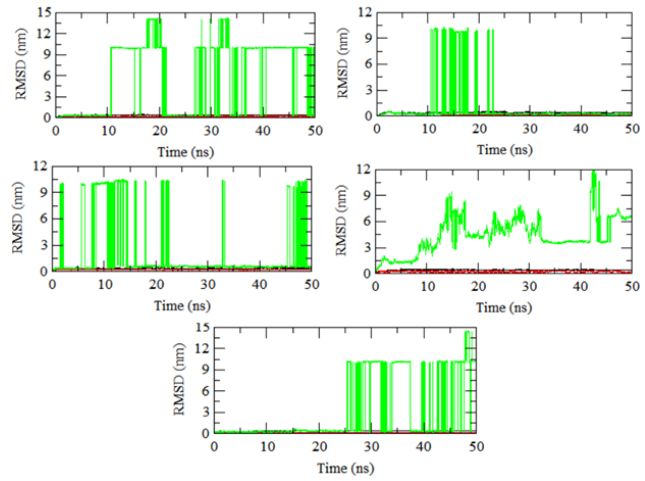


**Fig. 7. A-E.** The RMSD plot tracks structural alignment variations over time. Black, red, and green lines represent RMSD values of EphA2 protein backbone and reference inhibitors. A) EphA2-Dasatinib complex, B) EphA2-Mcule-1579910267 complex, C) EphA2-Mcule-3981378381 complex, D) EphA2-Mcule-1893218344 complex, and E) EphA2-Mcule-861769093

Mcule-8617639093.

### *3.4.6. Analyzing Principal Component Dynamics and Conformational Changes*

The Galaxy platform facilitated the application of Principal Component Analysis (PCA) to dissect the 50 ns trajectory of EphA2. The aim was to identify statistically significant conformations and unravel the key motions within the trajectory, specifically those responsible for conformational changes. This analysis provides crucial insights into the system dynamics. Through PCA, the primary motions inherent in the trajectory were unveiled, and those pivotal for eliciting conformational shifts were identified. Notably, non-periodic conformational alterations were highlighted in both Dasatinib and Mcule-8617639093, shown by two clusters along the dominant PC1 plane. This behavior, exhibiting global non-periodicity, was in contrast to Mcule-3981378381, where the PC1 variation was relatively low.

Quantitative assessment indicated that Mcule-8617639093 exhibited greater variation than Mcule-3981378381 and Dasatinib. The first three principal components collectively accounted for 37.9% of dasatinib, 27% of Mcule-3981378381, and 40.6% of Mcule-8617639093's total variance in the eigenvalue rank plot. PC1 was particularly significant for each compound, contributing 14.88%, 11.70%, and 16.18% of the variance for Dasatinib, Mcule-3981378381, and Mcule-8617639093, respectively (Figure 8 (A-C). Comparative exploration of the findings for Dasatinib, Mcule-3981378381, and Mcule-8617639093 (Figure 8 (A-C)) offers an in-depth understanding of their unique dynamic behaviors and provides valuable insights into the intricate molecular dynamics of EphA2, shedding light on the distinct conformational changes induced by various ligands. These insights can aid the design of targeted interventions and drug discovery strategies.

## 4. Discussion

During the course of conducting Structure-Based Virtual Screening (SBVS), we meticulously assessed over ten million compounds sourced from the MCULE digital archive of experimental ligands. Our systematic screening aimed to evaluate the binding affinity of these compounds to our target protein, resulting in the identification of a significant number of compounds with robust binding affinities. Notably, many of these compounds were previously unidentified as potential ligands for specific target proteins. To narrow the search for promising candidates, we subjected the compounds to toxicity and BOILED-Egg filtration, resulting in a refined list of only 37 compounds. This effective filtration process demonstrated the specificity of our search strategy for the exclusion of unrelated compounds. Comparing our findings to those of well-established inhibitors, we identified nine ligands displaying stronger binding propensities to EphA2. Molecular docking analysis highlighted common molecular interactions, such as van der Waals forces, conventional hydrogen bonds, carbon-hydrogen interactions, and alkyl interactions, shared between the potential inhibitor dasatinib and the top two ligands Mcule-3981378381 and Mcule-8617639093. Of particular interest, EphA2-Mcule-8617639093 exhibited enhanced stability compared to EphA2-Mcule-3981378381 and EphA2-Dasatinib in molecular docking simulations. This heightened stability was attributed to additional interactions, including pi-sulfur, pi-pi T-shaped, and unfavorable positive-positive interactions. These favorable interactions collectively contributed to an increased binding free energy, resulting in notable stability of the EphA2-Mcule-8617639093 complex, suggesting its potential for suppressing EphA2 overexpression.

Further investigations through Molecular Dynamics (MD) simulations have delved into the structural characteristics of these compounds. Parameters such as the Radius of Gyration (Rg) and Root Mean Square Deviation (RMSD) exhibited stability with minimal fluctuations in specific regions. Additionally, Surface Area of Solvent Accessibility (SASA) analysis indicated favorable solvent exposure, implying potential improvements in protein solubility and facilitation of protein-protein interactions. Principal Component Analysis (PCA) of the atomic movements underlying protein function revealed distinctive patterns, particularly in the case of Mcule-8617639093. Interestingly, this compound displayed the highest magnitude in the first principal component (PC1). Interestin-

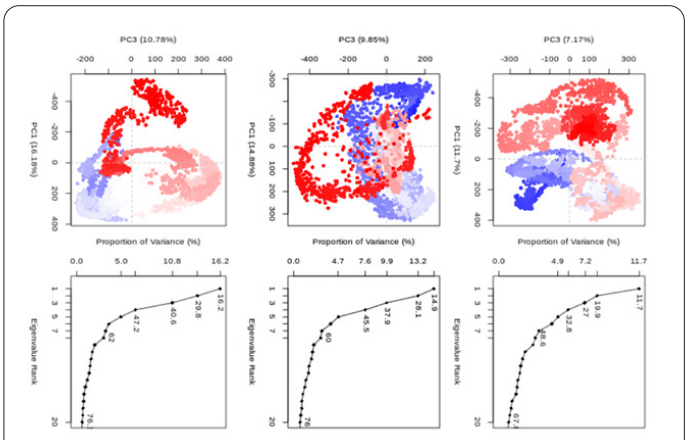


**Fig. 8. A-C.** Principal component analysis of EphA2 backbone Cα atom motions. A) Dasatinib, B) Mcule-3981378381, and C) Mcule-8617639093.

gly, all graphs indicate overlapping PC subspaces among the conformers, suggesting smooth transitions without significant energy barriers. Encouragingly, experimental testing for an established inhibitor demonstrated positive results for Mcule-8617639093, further validating its potential. Collectively, these findings suggest that Mcule-8617639093 is the most promising compound among the tested conformers. Subsequent in vitro studies are warranted to verify the inhibitory effects of this compound. Moreover, our SBVS efforts identified a potent compound, Mcule-8617639093, which demonstrated strong binding affinity and stability against EphA2. These findings hold significant promise for future therapeutic interventions and warrant further exploration and validation.

## 5. Conclusion

The study provides valuable insights into EphA2 overexpression using small molecules. Through the design and evaluation of a diverse series of 100 derivatives, our in silico assessment, particularly ADME prediction using SwissADME tools, proved instrumental in assessing the pharmacokinetic and pharmacodynamic attributes. These compounds exhibited promising pharmacological profiles, including favorable solubility, oral absorption, and bioavailability, suggesting their potential as effective drug candidates. Notably, the majority of compounds showed non-substrate status for P-glycoprotein, indicating potential evasion of efflux mechanisms, along with optimal log P values for blood-brain barrier penetration and hepatocyte intrinsic clearance. The prominence of Mcule-8617639093, aligning with computational findings and exhibiting favorable drug-like attributes, suggests its potential as a potent inhibitor. Experimental validation will be crucial to confirm the therapeutic utility of these compounds in addressing EphA2-associated conditions.

## Acknowledgments

The authors gratefully acknowledge the Research and Development Committee (RDC) of Integral University for generously providing the manuscript communication number (IU/R&D/2023-MCN0002010). Additionally, the authors would like to thank the DST-FIST funding (SR/FST/LS-1/2017/13(C)) for its support, which greatly contributed to the progress of this research.

## Conflict of Interests

The authors have no conflicts of interest to declare.

## Consent for publications

The author read and approved the final manuscript for publication.

## Ethics approval and consent to participate

No human or animals were used in the present research.

## Informed Consent

The authors declare that no patients were used in this study.

## Availability of data and material

All data supporting the findings of this study are provided within the manuscript.

## Funding

No funding was provided for this study.

## References

1. Amit I, Wides R, & Yarden Y (2007) Evolvable signaling networks of receptor tyrosine kinases: relevance of robustness to malignancy and to cancer therapy. Mol Sys Biol 3(1). https://doi.org/10.1038/msb4100195.
2. Baeten CIM, Hillen F, Pauwels P, de Bruine AP, & Baeten CGMI (2009) Prognostic Role of Vasculogenic Mimicry in Colorectal Cancer. Dis Colon Rectum 52(12): 2028–2035. https://doi.org/10.1007/DCR.0b013e3181beb4ff.
3. Brannan JM, Dong W, Prudkin L, Behrens C, Lotan R, Bekele BN, Wistuba I, Johnson FM (2009) Expression of the Receptor Tyrosine Kinase EphA2 Is Increased in Smokers and Predicts Poor Survival in Non–Small Cell Lung Cancer. Clin Cancer Res 15(13): 4423–4430. https://doi.org/10.1158/1078-0432.CCR-09-0473.
4. Cui X, Lee M, Yu G, Kim I, Yu H, Song E, Kim D (2010) EFNA1 ligand and its receptor EphA2: potential biomarkers for hepatocellular carcinoma. Int J Cancer 126(4): 940–949. https://doi.org/10.1002/ijc.24798.
5. Li X, Wang L, Gu JW, Li B, Liu WP, Wang YG, Zhang X, Zhen HN, Fei Z (2010) Up-regulation of EphA2 and down-regulation of EphrinA1 are associated with the aggressive phenotype and poor prognosis of malignant glioma. Tumour Biol 31(5): 477–488. https://doi.org/10.1007/s13277-010-0060-6.
6. Merritt WM, Kamat AA, Hwang JY, Bottsford M J, Lu C, Lin YG, Coffey D, Spannuth WA, Nugent E, Han LY, Landen CN, Nick AM, Stone RL, Coffman K, Bruckheimer E, Broaddus RR, Gershenson DM, Coleman RL, Sood AK (2010) Clinical and biological impact of EphA2 overexpression and angiogenesis in endometrial cancer. Cancer Biol Ther 10(12): 1306–1314. https://doi.org/10.4161/cbt.10.12.13582.
7. Nehal M, Khatoon J, Akhtar S, Khan MKA (2024) Exploring the potential of EphA2 receptor signaling pathway: a comprehensive review in cancer treatment. Mol Biol Rep 51(1): 337.
8. Udayakumar D, Zhang G, Ji Z, Njauw CN, Mroz P, Tsao H (2011) Epha2 is a critical oncogene in melanoma. Oncogene 30(50): 4921–4929. https://doi.org/10.1038/onc.2011.210
9. Tandon M, Vemula SV, Mittal SK (2011) Emerging strategies for EphA2 receptor targeting for cancer therapeutics. Expert Opin Ther Targets 15(1): 31–51. https://doi.org/10.1517/14728222.2011.538682.
10. Wilson K, Shiuan E, Brantley SDM (2021) Oncogenic functions and therapeutic targeting of EphA2 in cancer. Oncogene 40(14): 2483–2495. https://doi.org/10.1038/s41388-021-01714-8.
11. Wang H, Qiu W (2021) EPHA2 a promising therapeutic target for hepatocellular carcinoma. Mol Cell Oncol 8(3): 1910009. https://doi.org/10.1080/23723556.2021.1910009.
12. Wang H, Hou W, Perera A, Bettler C, Beach JR, Ding X, Li J, Denning MF, Dhanarajan A, Cotler SJ, Joyce C, Yin J, Ahmed F, Roberts LR, Qiu W (2021) Targeting EphA2 suppresses hepatocellular carcinoma initiation and progression by dual inhibition of JAK1/STAT3 and AKT signaling. Cell Rep 34(8): 108765. https://doi.org/10.1016/j.celrep.2021.108765.
13. Huang Z, Liu J, Zhang C, Yang X (2022) Lipofectamine 2000™ at transfection dose promotes EphA2 transcription in an HDAC4-dependent manner to reduce its cytotoxicity. Heliyon, 8(12): e12118. https://doi.org/10.1016/j.heliyon.2022.e12118.
14. Lévêque R, Corbet C, Aubert L, Guilbert M, Lagadec C, Adriaenssens E, Duval J, Finetti P, Birnbaum D, Magné N, Chopin V, Bertucci F, Le Bourhis X, Toillon RA (2019) ProNGF increases breast tumor aggressiveness through functional association of TrkA with EphA2. Cancer Lett 449: 196–206. https://doi.org/10.1016/j.canlet.2019.02.019.

15. Pratt RL, Kinch MS (2002) Activation of the EphA2 tyrosine kinase stimulates the MAP/ERK kinase signaling cascade. Oncogene 21(50): 7690–7699. https://doi.org/10.1038/sj.onc.1205758.
16. Zelinski DP, Zantek ND, Stewart JC, Irizarry AR, Kinch MS (2001) EphA2 overexpression causes tumorigenesis of mammary epithelial cells. Cancer Res 61(5).
17. Morris GM, Goodsell DS, Halliday RS, Huey R, Hart WE, Belew RK, Olson AJ (1998) Automated docking using a Lamarckian genetic algorithm and an empirical binding free energy function. J Comput Chem 19(14): 1639–1662. https://doi.org/10.1002/(SICI)1096-987X(19981115)19:14<1639::AID-JCC10>3.0.CO;2-B.
18. Bas DC, Rogers DM, Jensen JH (2008) Very fast prediction and rationalization of p K a values for protein–ligand complexes. Proteins 73(3): 765–783. https://doi.org/10.1002/prot.22102.
19. MU Azeem, S Akhtar, MH Siddiqui, MKA Khan (2021). Identification of Potential Lead Molecules against Dibenzo [a,l]pyrene-induced Mammary Cancer through Targeting Cytochrome P450 1A1, 1A2, and 1B1 Isozymes. Biointerface Res Appl Chem 12(1): 1096–1109. https://doi.org/10.33263/BRIAC121.10961109
20. Morris GM, Goodsell DS, Huey R, Olson AJ (1996) Distributed automated docking of flexible ligands to proteins: Parallel applications of AutoDock 2.4. J Comput Aided Mol Des 10(4): 293–304. https://doi.org/10.1007/BF00124499.
21. Nepstad I, Hatfield KJ, Grønningsæter IS, Aasebø E, Hernandez-Valladares M, Hagen KM, Rye KP, Berven FS, Selheim F, Reikvam H, Bruserud Ø (2019) Effects of insulin and pathway inhibitors on the PI3K-Akt-mTOR phosphorylation profile in acute myeloid leukemia cells. Signal Transduct Target Ther 4(1): 20. https://doi.org/10.1038/s41392-019-0050-0.
22. Mercurio FA, Pirone L, Di Natale C, Marasco D, Pedone EM, Leone M (2018) Sam domain-based stapled peptides: Structural analysis and interaction studies with the Sam domains from the EphA2 receptor and the lipid phosphatase Ship2. Bioorg Chem 80: 602–610. https://doi.org/10.1016/j.bioorg.2018.07.013.
23. Sun YL, Zhao YX, Guan YN, You X, Zhang Y, Zhang, M, Wu HY, Zhang WJ, Yao YZ (2023) Study on the Relationship Between Differentially Expressed Proteins in Breast Cancer and Lymph Node Metastasis. Adv Ther 40(9): 4004–4023. https://doi.org/10.1007/s12325-023-02588-w.
24. Ahmed Abousheishaa A, Hatim Sulaiman A, Zaman Huri H, Zaini S, Adha Othman N, bin Aladdin Z, Chong Guan N (2020) Global Scope of Hospital Pharmacy Practice: A Scoping Review. Healthcare 8(2): 143. https://doi.org/10.3390/healthcare8020143.
25. Kiss R, Sandor M, Szalai FA (2012) http://Mcule.com: a public web service for drug discovery. J Cheminform 4(S1): P17. https://doi.org/10.1186/1758-2946-4-S1-P17.
26. Poroikov VV (2020) Computer-Aided Drug Design: from Discovery of Novel Pharmaceutical Agents to Systems Pharmacology. Biochemistry (Moscow) Supplement Series B: Biomed khim 14(3): 216–227. https://doi.org/10.1134/S1990750820030117.
27. Ram Kumar A, Selvaraj S, Anthoniammal P, Jothi Ramalingam R, Balu R, Jayaprakash P, Sheeja MGP (2023) Comparison of spectroscopic, structural, and molecular docking studies of 5-nitro-2-fluoroaniline and 2-nitro-5-fluoroaniline: An attempt on fluoroanilineisomers. J Fluor Chem 270: 110167. https://doi.org/10.1016/j.jfluchem.2023.110167.
28. Khan MKA, Akhtar S, Arif JM (2018) Structural Insight into the Mechanism of Dibenzo[a,l]pyrene and Benzo[a]pyrene-Mediated Cell Proliferation Using Molecular Docking Simulations. Interdiscip Sci 10(4): 653–673. https://doi.org/10.1007/s12539-017-0226-7.
29. Ahmad KMK, Salman A, Al-Khodairy Salman F, Al-Marshad Feras M, Alshahrani Abdulrahman M, Arif Jamal M (2020) Computational Exploration of Dibenzo [a,l] Pyrene Interaction to DNA and its Bases: Possible Implications to Human Health. Biointerface Res Appl Chem11(4): 11272–11283. https://doi.org/10.33263/BRIAC114.1127211283.
30. Trott O, Olson AJ (2010) AutoDock Vina: Improving the speed and accuracy of docking with a new scoring function, efficient optimization, and multithreading. J Comput Chem 31(2): 455–461. https://doi.org/10.1002/jcc.21334.
31. Ajijur R, Salman A, Ahmad KMK. (2021) Combinatorial Design to Decipher Novel Lead Molecule against Mycobacterium tuberculosis. Biointerface Research Appl Chem 11(5): 12993–13004. https://doi.org/10.33263/BRIAC115.1299313004.
32. Khan MKA, Akhtar S, Arif JM (2018) Development of In Silico Protocols to Predict Structural Insights into the Metabolic Activation Pathways of Xenobiotics. Interdiscip Sci 10(2): 329–345. https://doi.org/10.1007/s12539-017-0237-4.
33. de Magalhães CS, Almeida DM, Barbosa HJC, Dardenne LE (2014) A dynamic niching genetic algorithm strategy for docking highly flexible ligands. Inf Sci 289: 206–224. https://doi.org/10.1016/j.ins.2014.08.002.
34. Ferreira GG, Quaresma ACS, Brandão DLN, Marinho AMR, Siqueira, JES, Correa KL, Silva-Júnior JOC, Percario S, Dolabela MF (2022) Evaluation of Genotoxicity and Toxicity of Annona muricata L. Seeds and In Silico. Molecules 28(1): 231. https://doi.org/10.3390/molecules28010231.
35. Khursheed A, Kumar Pandey A, Kumar Jain V (2023) ADMET Investigations On A Synthetic Derivative Of Genistein, And Molecular Docking Experiments Targeting Estrogen Receptor-α (ER-α) In The Pancreas. IJGASR 2(1): 18–40. https://doi.org/10.55938/ijgasr.v2i1.40.
36. Chen R, Hao X, Chen J, Zhang C, Fan H, Lian F, Chen X, Wang C, Xia Y (2023) Integrated multi-omics analyses reveal Jorunnamycin A as a novel suppressor for muscle-invasive bladder cancer by targeting FASN and TOP1. J Transl Med 21(1): 549. https://doi.org/10.1186/s12967-023-04400-3.
37. Santos KB, Guedes IA, Karl ALM, Dardenne LE (2020) Highly Flexible Ligand Docking: Benchmarking of the DockThor Program on the LEADS-PEP Protein-Peptide Data Set. J Chem Inf Mod. https://doi.org/10.1021/acs.jcim.9b00905.
38. Guedes IA, Costa LSC, dos Santos KB, Karl ALM, Rocha GK, Teixeira IM, Galheigo MM, Medeiros V, Krempser E, Custódio FL, Barbosa HJC, Nicolás MF, Dardenne LE (2021) Drug design and repurposing with DockThor-VS web server focusing on SARS-CoV-2 therapeutic targets and their non-synonym variants. Sci Rep 11(1): 5543. https://doi.org/10.1038/s41598-021-84700-0.
39. Venkateswara Rao B, Swain S, Siva B, Sasi Priya SVS, Jadav SS, Jain N, Ramalingam V, Suresh Babu K (2023) Novel heterocyclic analogues of bergenin as anti-mitotic agents: Design, synthesis, biological evaluation and molecular docking study. J Mol Str 1280: 135048. https://doi.org/10.1016/j.molstruc.2023.135048.
40. Zoete V, Grosdidier A, Cuendet M, Michielin O (2010) Use of the FACTS solvation model for protein-ligand docking calculations. Application to EADock. J Mol Recognit 23(5): 457–461. https://doi.org/10.1002/jmr.1012.
41. Khan FI, Lai D, Anwer R, Azim I, Khan MKA (2020). Identifying novel sphingosine kinase 1 inhibitors as therapeutics against breast cancer. J Enzyme Inhib Med Chem 35(1): 172–186. https://doi.org/10.1080/14756366.2019.1692828.
42. Vanommeslaeghe K, Hatcher E, Acharya C, Kundu S, Zhong S, Shim J, Darian E, Guvench O, Lopes P, Vorobyov I, Mackerell AD (2010) CHARMM general force field: A force field for drug-like molecules compatible with the CHARMM all-atom additive biological force fields. J Comput Chem 31(4): 671–690. https://

doi.org/10.1002/jcc.21367.
43. Lemkul JA (2020) Pairwise-additive and polarizable atomistic force fields for molecular dynamics simulations of proteins. Prog Mol Biol Transl Sci (pp. 1–71): https://doi.org/10.1016/bs.pmbts.2019.12.009.
44. Vanommeslaeghe K, MacKerell AD (2012) Automation of the CHARMM General Force Field (CGenFF) I: Bond Perception and Atom Typing. J Chem Inf Mod 52(12): 3144–3154. https://doi.org/10.1021/ci300363c.
45. Gonçalves YMH, Senac C, Fuchs PFJ, Hünenberger PH, Horta BAC (2019) Influence of the Treatment of Nonbonded Interactions on the Thermodynamic and Transport Properties of Pure Liquids Calculated Using the 2016H66 Force Field. J Chem Theory Comput 15(3): 1806–1826. https://doi.org/10.1021/acs.jctc.8b00425.
46. Gonçalves YMH, Senac C, Fuchs PFJ, Hünenberger PH, Horta BAC (2019) Influence of the Treatment of Nonbonded Interactions on the Thermodynamic and Transport Properties of Pure Liquids Calculated Using the 2016H66 Force Field. J Chem Theory Comput 15(3): 1806–1826. https://doi.org/10.1021/acs.jctc.8b00425.
47. Bilsland AE, McAulay K, Wes R, Pugliese A, Bower J (2021) Automated Generation of Novel Fragments Using Screening Data, a Dual SMILES Autoencoder, Transfer Learning and Syntax Correction. J Chem Inf Mod 61(6): 2547–2559. https://doi.org/10.1021/acs.jcim.0c01226.
48. Egan WJ, Merz KM, Baldwin JJ (2000) Prediction of Drug Absorption Using Multivariate Statistics. J Med Chem 43(21): 3867–3877. https://doi.org/10.1021/jm000292e.
49. Egan WJ, Lauri G (2002) Prediction of intestinal permeability. Adv Drug Deliv Rev 54(3): 273–289. https://doi.org/10.1016/S0169-409X(02)00004-2.
50. Attique S, Hassan M, Usman M, Atif R, Mahboob S, Al-Ghanim K, Bilal M, Nawaz M (2019) A Molecular Docking Approach to Evaluate the Pharmacological Properties of Natural and Synthetic Treatment Candidates for Use against Hypertension. Int J Environ Res Public Health 16(6): 923. https://doi.org/10.3390/ijerph16060923.
51. O'Boyle NM, Banck M, James CA, Morley C, Vandermeersch T, Hutchison GR (2011) Open Babel: An open chemical toolbox. J Cheminform 3(1): 33. https://doi.org/10.1186/1758-2946-3-33.
52. Ertl P, Rohde B, Selzer P (2000) Fast Calculation of Molecular Polar Surface Area as a Sum of Fragment-Based Contributions and Its Application to the Prediction of Drug Transport Properties. J Med Chem 43(20); 3714–3717. https://doi.org/10.1021/jm000942e.
53. Lipinski CA, Lombardo F, Dominy BW, Feeney PJ (2012) Experimental and computational approaches to estimate solubility and permeability in drug discovery and development settings. Adv Drug Deliv Rev 64(SUPPL) 4–17: https://doi.org/10.1016/j.addr.2012.09.019.
54. Veber DF, Johnson SR, Cheng HY, Smith BR, Ward KW, Kopple KD (2002) Molecular Properties That Influence the Oral Bioavailability of Drug Candidates. J Med Chem 45(12): 2615–2623. https://doi.org/10.1021/jm020017n.
55. Ghose AK, Viswanadhan VN, Wendoloski JJ (1999) A Knowledge-Based Approach in Designing Combinatorial or Medicinal Chemistry Libraries for Drug Discovery. 1. A Qualitative and Quantitative Characterization of Known Drug Databases. J Comb Chem 1(1): 55–68. https://doi.org/10.1021/cc9800071.
56. Muegge I, Heald SL, Brittelli, D. (2001). Simple Selection Criteria for Drug-like Chemical Matter. J Med Chem 44(12), 1841–1846. https://doi.org/10.1021/jm015507e
57. Ali J, Camilleri P, Brown M B, Hutt AJ, Kirton SB (2012) Revisiting the General Solubility Equation: In Silico Prediction of Aqueous Solubility Incorporating the Effect of Topographical Polar Surface Area. J Chem Inf Mod 52(2): 420–428. https://doi.org/10.1021/ci200387c.
58. Daina A, Michielin O, Zoete V (2017) SwissADME: a free web tool to evaluate pharmacokinetics, drug-likeness and medicinal chemistry friendliness of small molecules. Sci Rep 7(1): 42717. https://doi.org/10.1038/srep42717.
59. Potts RO, Guy RH (1992) Predicting Skin Permeability. Pharm Research 9(5): 663–669. https://doi.org/10.1023/A:1015810312465.
60. Khan MKA, Alouffi S, Ahmad S (2023) Identifying potential inhibitors of C-X-C motif chemokine ligand10 against vitiligo: structure-based virtual screening, molecular dynamics simulation, and principal component analysis. J Biomol Struct Dyn 1–18: https://doi.org/10.1080/07391102.2023.2242952.
61. Ali S, Khan F, Mohammad T, Lan D, Hassan M, Wang Y (2019) Identification and Evaluation of Inhibitors of Lipase from Malassezia restricta using Virtual High-Throughput Screening and Molecular Dynamics Studies. Int J Mol Sci 20(4): 884. https://doi.org/10.3390/ijms20040884.
62. Kuzmanic A, Zagrovic B (2010) Determination of Ensemble-Average Pairwise Root Mean-Square Deviation from Experimental B-Factors. Biophys J 98(5): 861–871. https://doi.org/10.1016/j.bpj.2009.11.011.